Development of Multilayer Structures for Biosensors Based on SPR

Final Report

By:
ADIR HAZAN

Supervisors:
Dr. Alina Karabchevsky & Dr. Moshe Zohar

SCE
SHAMOON COLLEGE OF ENGINEERING

 # 108

Shamoon College of Engineering

Department of Electrical and Electronics Engineering

Beer Sheva

Development of Multilayer Structures for Biosensors Based on Surface Plasmon Resonance

Author:
Adir Hazan

Supervisors:
Dr. Alina Karabchevsky
Dr. Moshe Zohar

Final Report

An engineering project submitted in fulllment of the requirements for the degree of Bachelor of Science

June, 2019

SCE
SHAMOON COLLEGE OF ENGINEERING

I, Adir Hazan, hereby declare that the project work entitled as "Development of Multilayer Structures for Biosensors Based on Surface Plasmon Resonance" is an authentic record of my own work, which was carried out at *'Light-on-a-Chip'* research group leading by Dr. A. Karabchevsky, in Electrooptics and Photonics Engineering Department, Ben-Gurion University, Beer-Sheva. This engineering project submitted in fulllment of the requirements for the degree of Bachelor of Science (*B.Sc.*) in Electrical and Electronics Engineering under the guidance of both Dr. Alina Karabchevsky and Dr. Moshe Zohar.

Type of project: Research.

Project Areas: Integrated Photonics, Plasmonics, Optical Biosensors, Nanotechnology, Infrared Spectroscopy.

Approved By:

Alina Karabchevsky

Dr. Alina Karabchevsky,
Electrooptics and Photonics
Engineering Department, BGU

Moshe Zohar

Dr. Moshe Zohar,
Electrical and Electronics
Engineering Department, SCE

Adir Hazan

Adir Hazan, Author

Acknowledgments

I would first like to acknowledge to both of my supervisors, Dr. Alina Karabchevsky and Dr. Moshe Zohar, for the useful remarks and engagement through the learning process of this project, which have inspired me to thrive for excellence. It has been great working with you, and I hope to work with you again in the future.

Furthermore, I would like to express my deep appreciation and gratitude to my supervisor, Dr. Alina Karabchevsky, for the support she provided to me all the way, the sharing of expertise, valuable guidance, and access to the laboratory and research facilities. Without her precious support, it would not be possible to conduct this project. The door to Dr. Karabchevsky office was always open whenever I ran into a trouble spot or had a question. Thank you for introducing me to the fascinating Photonics world.

The assistance provided by all members in '*Light-On-a-Chip*' group was invaluable to the success of my project, and I would like to thank for their friendship and encouragement.

Abstract

This project presents the development of multilayer structures for molecular detection and biosensing based on surface plasmon resonance (SPR). By designing and engineering multilayer structures on the nanometer scale, one can utilize SPR features to increase the molecular vibrational transitions in the near-infrared region. This work covered investigating, design, fabrication, and demonstration of a plasmonics structure used for sensing by applying the SPR properties.

The primary component of the optical system is the chip sensor. Based on the current methodology a near-guided wave SPR (NGWSPR) biosensor was developed. This obtained with implementing a modification to the conventional structure of the Kretschmann-Raether, with thin dielectric over-layer. Achieving optimal system performance is a major consideration in sensor design. Following simulations results, the NGWSPR sample was fabricated with electron beam physical vapor deposition (EBPVD) process. Finally, the system must be tested, thus experiment and measurements have to take place and compared with the numerical models.

One can support guided optical waves in this model by introducing a thick enough dielectric layer, so-called GWSPR configuration, which less known in the methodology. The last step of this work is to examine theoretically the possibility of GWSPR model for detection molecular vibrational transitions overtones using surface-enhanced infrared absorption (SEIRA) technique.

For future continuation of the project, Dr. A. Karabchevsky and I investigated the hybrid-dielectric optical system consist of gold nanorods on the top surface of GWSPR configuration. We demonstrated this system for real-time all-optical switch engineered to operate at optical telecommunication wavelengths. Our discovery may open the door for miniature, affordable and ultrafast chip-scale polarization switches as compared to the traditional electronic switches. Due to the impact of this discovery, the work will participate in two conferences and will be submitted in these days to the prestigious journal publishing *Nature Photonics*.

Keywords: plasmonic structures, optical-biosensor, surface plasmon resonance, infrared spectroscopy.

CONTENTS

LIST OF FIGURES

LIST OF ABBREVIATIONS

DA	**D**ifferential **A**bsorption
EBPVD	**E**lectron **B**eam **P**hysical **V**apor **D**eposition
EM	**E**lectro **M**agnetic
ESP	**E**xtended **S**urface **P**lasmon
FWHM	**F**ull **W**idth **H**alf **M**aximum
GWSPR	**G**uided-Wave **S**urface **P**lasmon **R**esonance
IR	**I**nfra **R**ed
KR	**K**retschmann - **R**aether
LOD	**Lo**w **D**detection limit
LSPR	**L**ocalized **S**urface **P**lasmon **R**esonance
NGSPR	**N**ear **G**guided **W**ave **S**urface
NIR	**N**ear **I**nfra **R**ed
NMA	**N** - **M**ethyl**a**niline
RI	**R**efractive **I**ndex
SEIRA	**S**urface **E**nhanced **I**nfrared **A**bsorption
SNR	**S**ignal to **N**oise **R**atio
SPR	**S**urface **P**lasmon **R**esonance
SPW	**S**urface **P**lasmon **W**ave
TE	**T**ransverse **E**lectric
TIR	**T**otal **I**nternal **R**eection
TM	**T**ransverse **M**agnetic

CHAPTER 1

INTRODUCTION

1.1 Motivation

Since biosensors have become an important part of our daily life, an extended interest among researchers, engineers, and industrial companies in the field of improving available devices and developing new tools. In particular, optical biosensor represents the most popular kind of biosensor due to their immune to electromagnetic (EM) interference, real-time detection, sensitivity, small size, can provide qualitative information, and allow multiple detections within a single device[1;2;3]. Their advantages lead to a wide range of applications in healthcare, drug discovery, biomedical research, environmental monitoring, food control, etc.

Infrared (IR) absorption spectroscopy is a powerful technique for investigating structural, functional, and compositional changes in biomolecules[4]. It is possible to identify molecular bonds signature not only by the fundamental vibrational transitions but also by the higher harmonics of the fundamental molecular vibrational transitions, so-called overtones[5;6]. While fundamental vibrational transitions of organic molecules appear in the mid and far IR regions, overtones can observe in the near-IR where affordable equipment is required which lead to low-cost devices. However the intensities of the overtones are a few orders smaller relative to the intensities of the fundamental transitions, therefore it more difficult to detect them. Several attempts were done to enhance the cross-section of the vibrational transitions overtones[7;8] but detect them still considered mysterious.

In order to increase the sensitivity of IR absorption spectra, one can use the characteristics of the SPR phenomenon by engineering multilayer structures on the nanometer scale[9]. Currently, SPR is a well-established technology for label-free detection

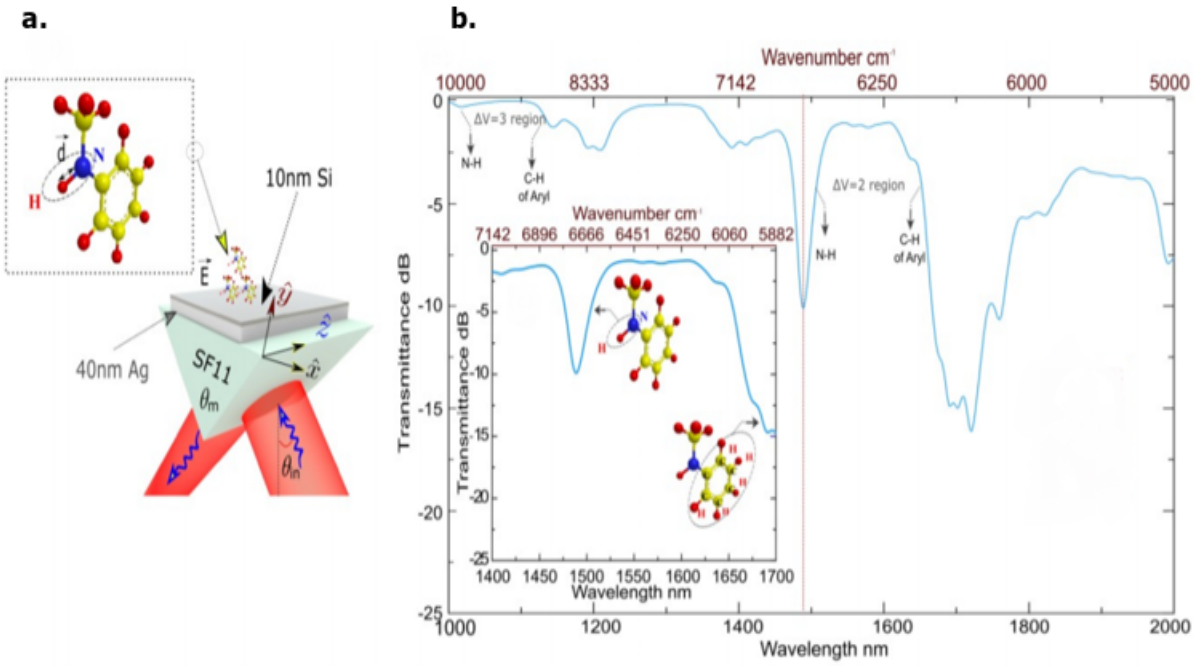

Figure 1.1: Transmittance spectra of NMA using NGWSPR model[8]: (a) the NGWSPR model based on KR configuration with the probing molecule. **(b)** transmittance spectra of NMA in hexane mixture and zoomed at the 1^{st} overtone region of N-H and C-H bands.

in the markets. SPR is a collective oscillation of free charges, conduction electrons, present at the interface of two media metal–dielectric with permittivities of opposite signs due to excitation of light[10]. It is the fundamental principle behind many biosensor applications and the basis of many conventional tools for measuring adsorption of material on a metal surface typically gold or silver[11;12;13;14] or on a surface of metal nanoparticles[15;16;17].

1.2 Concepts

Design of an SPR biosensor was presented in this work based on two concepts. On the one hand, develop an NGWSPR multilayer biosensor for sensing and test it with the refractive index (RI) detection method. On the other hand, examine the utilizing of GWSPR configuration with SEIRA technique for molecular overtone detection. Both of the multilayer structure models are based on improving the conventional Kretschmann-Raether (KR) configuration.

Treating SPR physically starts from calculating the dispersion relation of surface plasmon waves from a smooth layer that can be excited in specific structures. The analytical model of SPR biosensor in the literature[18;19] allow engineering of NGWSPR

structure as shown in Figure 1.1.a[8]. Measuring the changes in the reflected light from the structure due to the RI changes induced by the molecular interactions can be utilized for sensing. Through this work, a numerical tool was designed in Matlab environment for sensing water using the NGSPR configuration. Achieving optimal performance could be obtained with increasing the signal to noise ratio (SNR) by maximizing the efficiency of the exciting surface plasmon wave with the required wavelength.

Simulations of the complete optical system were produced with Comsol Multiphysics software. Based on the results of numerical tools, a chip was fabricated in Nano-Fabrication center at Ben-Gurion university by EBCVD process. Then, an experiment with the fabricated samples took a place at '*Light-on-a-Chip*' research laboratory to test the optical biosensor. Analysis of the results allows calibrating the optical system with the designed numerical tools, which covered the change in the optical properties of the materials by the deposition process.

In the case of IR absorption spectroscopy, the absorption spectra of organic molecules are characterized by a series of bands, directly linked to the molecular vibrational modes[5;6]. Figure 1.1.b[8] shows the transmittance spectra of N-Methylaniline (NMA) probing molecule in hexane mixture using NGSPR model, at the 1^{st} and 2^{nd} overtones regions of N-H and C-H bands. When tuning the surface plasmon to resonate at a specific vibrational overtone frequency of the molecule, as a consequence the IR absorption spectra of the vibrational increases.

Engineering of GWSPR configuration for overtone detection with SEIRA technique achieved with quantifying the absorption of the vibrational transition overtone due to the interaction with the plasmonic field coupled to guided waves in the dielectric film. One can recognize the absorption feature of the interrogated overtone by calculating the differential absorption which simplified by[7]:

$$\triangle A = \frac{A_{molecule}}{A_{background}} \tag{1.1}$$

this obtained when collecting the reflected light from the multilayer structure when the molecule is present on the top surface as a semi-infinite medium, and next collect the reflected light when considering only the background refractive index which is the absorption caused only by the plasmonic field when the vibrational transitions of the molecule are deactivated.

CHAPTER 2

LITERATURE SURVEY

Engineering of plasmonic structures on the nanometric scale considered a future milestone of optic science. These structures are very useful in a variety of fields, especially in biosensing. The nanostructure of material can affect its properties in many ways, in particular, in the way it interacts with light. By creating structures which are controlled on a length scale below the wavelength of the incident radiation, namely, a matter on a scale much smaller than the wavelength of visible light, this radiation can be manipulated. The light interaction with conducting electron density of metals or semiconductors enhances exotic features which lead to advanced technologies[20;21;22].

2.1 Optical Biosensors

Optical biosensors utilize the effects induced by light in a specific structure to detect a target molecule. The general steps in optical biosensor design can be described with Figure 2.1.a[23]. The mechanism starts from optical transducers, which required to select a detection method and supported optical nanostructure. Next, need considering the chemistry interface between the biosensor and the target molecule. The last step is the signal processing, through convert and amplification the optical signal to an electric signal directly to signal analytical system for analyzing the results.

Biosensor commercialization is not so simple, due to high costs, problems of stability and sensitivity, quality assurance, and the impact of competing technologies. Thus, required biosensors which capable detect very low levels of a high number of chemical and biochemical substances. Ideally, need to obtain the fabrication of optical biosensors with the several features: very highly sensitive and selective, capable of simultaneous multi-analytical material determination, ultrafast, stable, simple to operate, robust, cheap

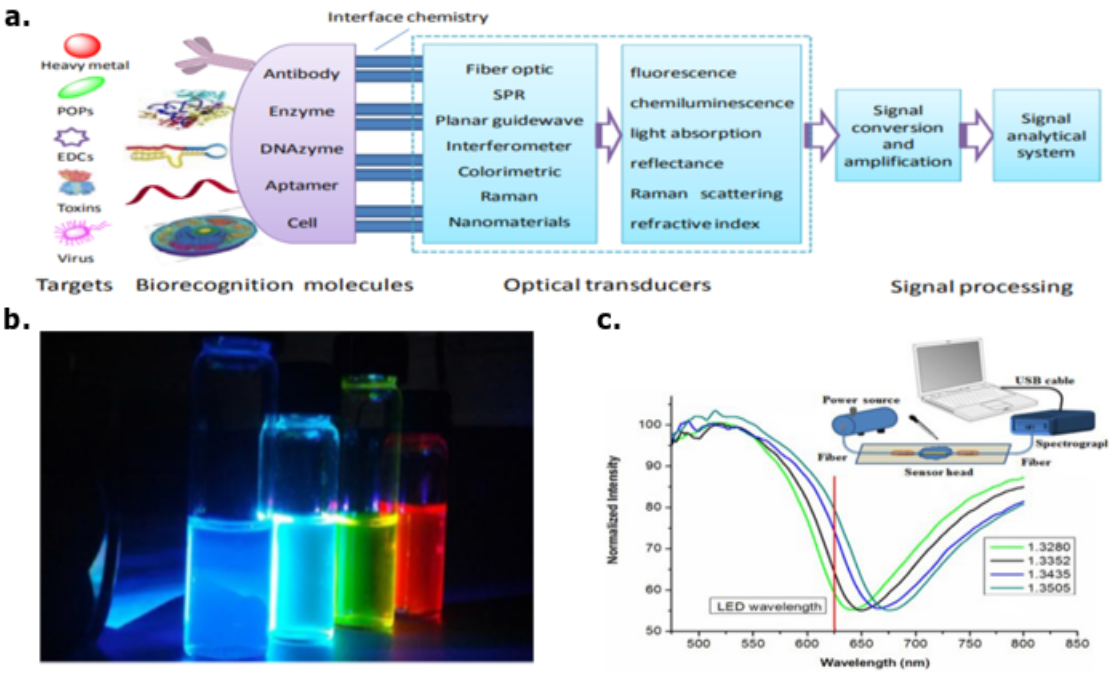

Figure 2.1: Optical biosensors: **(a)** schematic of an optical biosensor[23]. **(b)** fluorescent dyes and polymers in the lab of J. Yang[24]. **(c)** experiment setup for measuring the absorption spectra of the optic fiber SPR sensor[25].

and small size device[1]. Optical sensors represent the most common type of biosensor due to their particularly immune to EM interference, sensitivity, ultrasmall, low cost, and can provide multiple detections within a single device. Furthermore, provide qualitative information and have great potential for direct and real-time detection of many chemical and biological substances. Due to the increasing quantity of commercially available devices, it is possible to testify their success[3].

In general, there are two detection protocols that can be implemented in optical biosensing: fluorescence-based detection and label-free detection. In fluorescence detection, either target molecules or biorecognition molecules are labeled with fluorescent tags, such as dyes as shown in Figure 2.1.b[24]. The intensity of the fluorescence indicates the presence of the target molecules, and the strength of the interaction between target and biorecognition molecule[26;24]. On the other hand, in the label-free detection method no labeling processes are needed, molecules are detected in their natural forms. Label-free use the changes in optical properties to sense the target molecule which is relatively easy and cheap to perform. Therefore there is no need for large volumes of samples. This feature gives the label-free detection methods advantageous when ultrasmall volumes of the sample are presented[2;25]. Figure 2.1.c[25] illustrate a label-free detection measurement by plotting the wavelength dependence of the light intensity from the optical biosensor.

Even small changes of RI induced by molecular interactions yield different results in the spectrum, leading to the sensing ability of various analytical materials.

There are several detection methods under label-free optical detection, this work focuses on two of them: RI detection method, and optical absorption detection method. They reflect the optical properties of the medium to be sensed by altering the optical signal[25;8]. One of the most other widely known methods is Raman spectroscopic detection which is unique. On one hand, the target does not need to be labeled, but on the other hand, the scattered Raman emission used in the same manner as a fluorescence for detection[27].

In addition, some of the optical structures that are widely used for sensing are (i) SPR (ii) optical waveguide[28;29] (iii) optical ring resonators[30] (iv) optical fiber[31] (v) photonic crystal[32]. (vi) structures for fluorescence and surface-enhanced Raman scattering[27], and other structures are evolving. Through this work, the development of optical biosensor performed based on the design of SPR multilayer structure due to its advantages.

2.2 Infrared Spectroscopy

Spectroscopy deals with the interaction between light and matter. Due to variations in molecular energy, this interaction causes absorption[33] or emission of radiation. The energy appears in different regions of the EM spectrum and gives unique information about the molecular structure. IR is the region of the EM radiation spectrum, invisible to the human eye, where wavelengths range from about $700nm$ to $1mm$. It covers a range of techniques, mostly based on absorption spectroscopy which can be used to identify chemicals and biomolecules structure[5]. IR used in a variety of applications, among the most well-known are heat sensors, thermal imaging and night vision equipment which based on thermal molecular transitions.

IR classified into several spectral regions, also called bands, typically separated into near-, mid- and far-infrared. The mid-IR band covers wavelengths ranging from $1,300nm$ to $3\mu m$. Whereas wavelengths in the far-IR band, which are closest to microwaves, extend from $3\mu m$ to $1mm$. In this regions, the absorption spectra of organic molecules are characterized by a series of bands, directly linked to the vibrational modes. Fundamental vibrational transitions of organic molecules are typically in the range of $3-20\mu m$, so-called the fingerprint region. Theoretically, spectroscopic transitions happen at well-defined frequencies which leading to absorption lines with zero frequency width. However, in reality, the mechanisms such as lifetime and Doppler broadenings endow measured different shape absorption lines directly related to the absorption coefficient and dielectric function of the molecule[6]. Therefore, IR absorption spectroscopy is a great technique for molecular detection and sensing. One can be found in Appendix. A1, for deep

understanding, an example of diagrams of an oscillator mechanism described by the energy levels, and the corresponding spectral transmittance patterns. In addition, showing the general principle of EM radiation absorption.

Since in the mid-IR region, bulky and expensive equipment is needed, molecular fingerprints can be also deduced from the higher harmonics of vibrational transitions named overtones which appear in the near-infrared and has been efficiently detected by Karabchevsky et. al.[7;8]. The near-IR band contains the range of wavelengths closest to the red end of the visible light spectrum. It is generally considered to consist of wavelengths measuring from $750nm$ to $1,300nm$. Because of its traditional usage for optics telecommunication, this region benefits from affordable powerful sources, low propagation losses, and high coupling efficiency compatible with silica fibers[31]. However the intensities of the molecular vibrational overtones are a few orders smaller relative to the intensities of the fundamental transitions, therefore it more dicult to detect them.

When light is incident on the nanoscale metallic films, traditionally, made of silver or gold, one can excite plasmonic resonances which cause to enhance the electric field that leading to increasing the sensitivity of infrared absorption spectra. Increasing the signal with field enhancement is the basis for SEIRA spectroscopy. The field enhancement is normally achieved by exciting the localized surface plasmon resonances in the mid-IR region. Then, it is possible to consider the power absorbed by a material with a small imaginary part of its dielectric constant, which simplified by[8]:

$$P_{Abs} = \frac{\omega}{2} Im(\varepsilon)|E|^2 \tag{2.1}$$

where E, $|E|^2$, and ω are the electric field in the material, the absorption signal scales with the intensity, and the frequency, respectively.

Composite plasmonic waveguide structures shown by Karabchevsky et al.[28] enable plasmonic filed confinement to the metal film, through this work, the utilizing of GWSPR conguration with SEIRA spectroscopy for molecular overtone detection examined. In detail, enhance the vibrational transitions overtones in the near-IR by utilizing the propagating surface plasmons coupled to guided waves in the dielectric film. Therefore they can be detected easily by measuring the absorption spectra of the molecule.

2.3 Surface Plasmon Resonance

SPR is a collective oscillation of free charges, conduction electrons, present at the interface of two media metal–dielectric with permittivities of opposite signs due to excitation of light[10]. SPR can exist in specific structures on the nanometric scale.

In general, plasmons for noble metal nanostructures can be classified into two forms: propagating (or extended) surface plasmons (ESPs), and localized surface plasmon

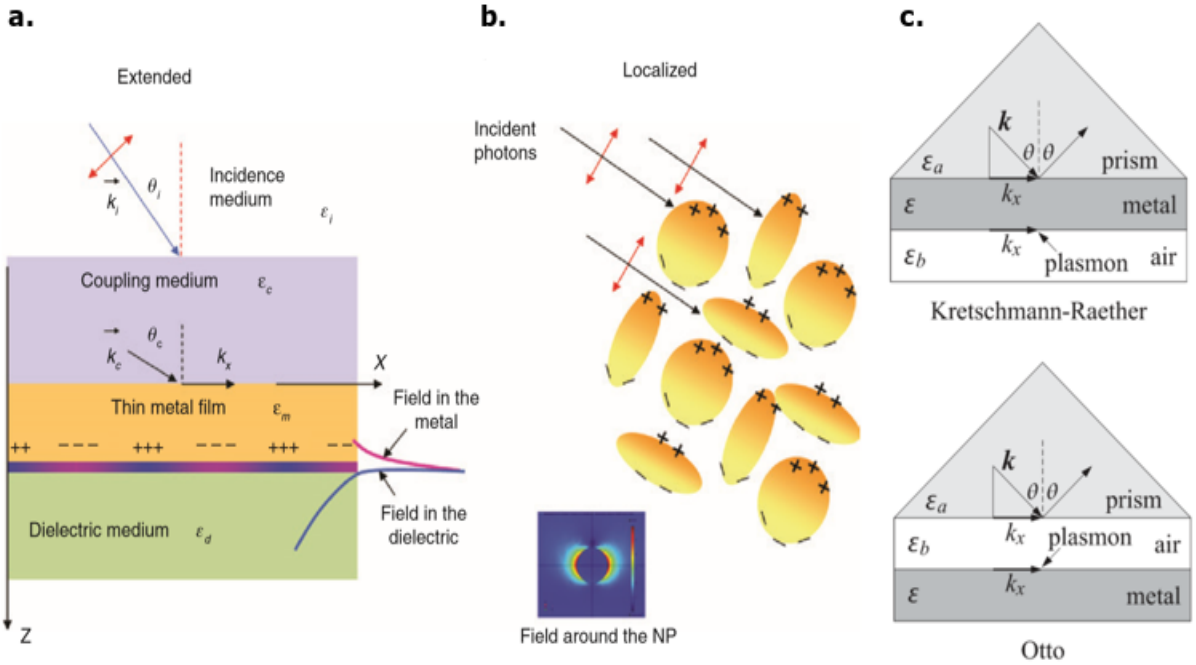

Figure 2.2: General excitation schemes for extended and localized surface plasmons: **(a)** exciting ESPs through a coupling medium.[34] **(b)** exciting LSPs by direct excitation from free space.[34]. **(c)** KR and Otto configurations. The wave is evanescent perpendicular to the interface, and therefore, the field is enhanced at the interface. The field penetrates the metal only within the skin depth, whereas in the dielectric, it can be from a few hundreds of nanometers until a few microns.[18].

resonances (LSPRs). In LSPRs case, plasmons are sustained by nanoparticles much smaller than the incident wavelength give rise to intense absorption, scattering, and extremely enhanced EM fields at their resonance wavelengths. The most used technique for illustrating the exciting LSPs is by directly shining a light on a collection of metal nanoparticles on a substrate, as shown in Figure 2.2.a[34]. Contrast to the ESPs case, light does not need to be polarized as the excitation occurs due to the scattering. Additional, as a consequence the field distributions enhanced around the nanoparticles.

On the other hand, Figure 2.2.b[34] shows ESPs excited at the interface of two media metal–dielectric with permittivities of opposite signs due to excitation of transverse magnetic (TM) polarized light through a coupling medium. Actually, the coupling medium used to match the momentum of a photon with that of surface plasmon in KR configuration. It can be various options such as a prism, waveguide, grating, or optical fiber. The ESPs travel along the metal-dielectric interface and the fields decaying exponentially into both bounding mediums. Their wavenumber k_x of propagation along the interface is larger than in the free-space value at the same frequency. Therefore, such

plasmons cannot couple directly to plane waves incident on the interface. However, if the incident TM plane wave is from a dielectric and from an angle that is greater than the angle of total internal reection (TIR)[18], then the corresponding wavenumber will be greater than its vacuum value and it could excite a plasmon wave along the interface.

Typically, ESPs supported by structures with at least one dimension approaching the excitation wavelength, namely, thin metal films attached to the coupling medium. Two of the most widely used structures where ESPs can be excited are the KR configuration and Otto configuration, which both shown inFigure 2.2.c[18]. Clearly shown that KR configuration is more practical to fabricate model than Otto due to the air gap. A surface wave is excited due to attenuated TIR of the light at the interface between the metal and dielectric.

The excitation of plasmons by TM-polarized coherent light requires a prism which matches between the wavevector k of the incidence light and the wavevector of the plasma[18]:

$$\sqrt{\varepsilon_p} sin\theta_p = Re\left\{\sqrt{\frac{\varepsilon_m \varepsilon_a}{\varepsilon_m + \varepsilon_a}}\right\} \tag{2.2}$$

where ε_p is the dielectric constant of the prism, which simplified by: $k_x = \sqrt{(\varepsilon_p)}(\omega/c)sin\theta_p$ while c, ω, ε_m, and ε_a are the light velocity in free space, the angular frequency, the complex dielectric constants of the metal and analyte, respectively. The relative dielectric constant ε_i and the RI n_i of each media are related by $\varepsilon_i = n_i^2$. The lossless dielectric will do as long as it satises $n_a < n_p$. The TIR angle is $sin\theta_c = n_a/n_p$, and the angle of incidence from the prism side is required to be $\theta > \theta_c$[18]. According to Equation 2.2 the SPP can be excited at a specific angle depending on the light wavelength through the materials dispersion relation. This model allows measured the reflectivity from the structure as a function of the angle of incidence or wavelength of incident light so-called wavelength interrogation.

2.3.1 The Field Distribution

Engineering of NGWSPR configuration requires to treat SPR phenomenon physically, namely, calculating the dispersion relation of surface plasmons waves that can be excited in specific structures. Therefore extensive surveys of the literature included algorithms for calculating field distribution in N layered structure[18;19;35]. During this work, the general structure constitutes an NGWSPR sensor, which considering the general case of plane wave radiation interacting with N thin-films between two semi-infinite medium. Figure 2.3 show the equivalent optical system of a multilayer structure used for sensing. Assuming that the interfaces between the media are flat and the layers are homogenous and isotropic. The construction parameters comprise the RI n_j and the thicknesses d_j

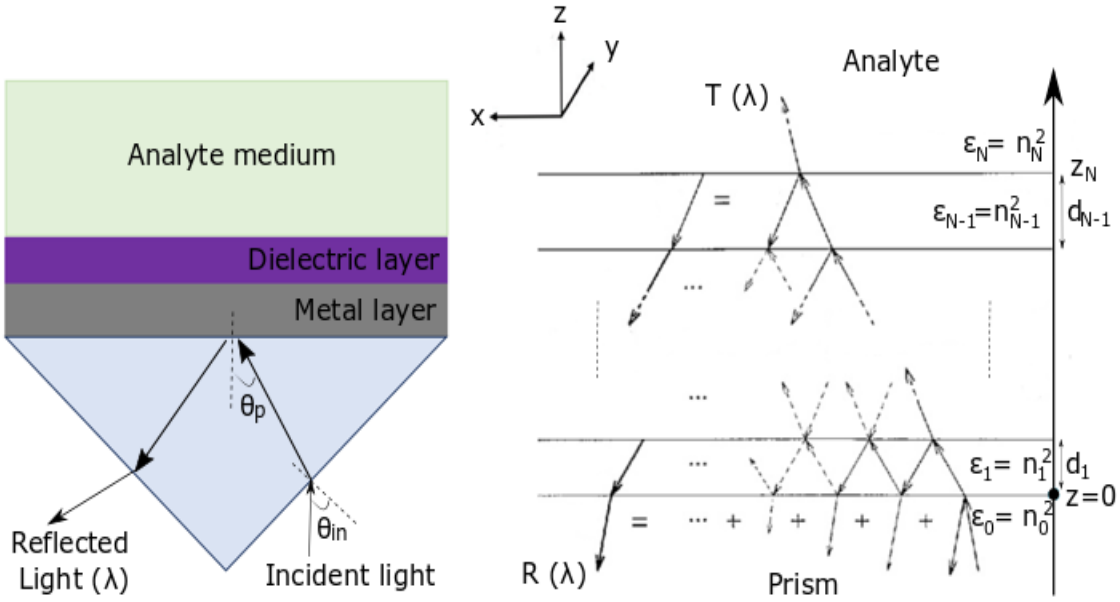

Figure 2.3: Field distribution in multilayer structure: the NGWSPR configuration (left) and equivalent optical system in the general case (right) corresponding to the interaction of plane wave with a multilayer structure, which composed of N homogenous and isotropic thin layers with $(N+1)$ interfaces that bounded by semi-infinite homogenous and isotropic mediums.

of each layer $j = 1, 2, \ldots, N$ as well as the RI n_p and n_a of the incident medium, in our case it is the prism, and the analyte medium. On the other hand, further required to consider the external variables of the optical system, in particular, the incident angle θ, the wavelength λ, and the polarization of the incident radiation.

One can calculate the intensity of reflected light and transmitted light through the multilayer structure, but our interest, in this case, is to obtain the reflectance of the system. The most used method for calculating the reflectance $R = |\Gamma|^2$ of a multilayer structure is based on a matrix formulation of the boundary conditions at the film surfaces derived from Maxwell's equations, namely, calculating the EM fields distribution in the structure. The reflection coefficient of a multilayer structure consisting of N layers bounded by semi-infinite medium is defined by[19]:

$$\Gamma = \frac{\eta_p \mathbf{E}_p - \mathbf{H}_p}{\eta_p \mathbf{E}_p + \mathbf{H}_p} \tag{2.3}$$

where the electric and magnetic vectors in the incident medium given by:

$$\begin{pmatrix} \mathbf{E}_p \\ \mathbf{H}_p \end{pmatrix} = \mathbb{M} \begin{pmatrix} 1 \\ \eta_p \end{pmatrix} \tag{2.3a}$$

$\mathbb{M}$ is a product matrix which represents the j^{th} films of the structure. It can easily solve with a general transfer-matrix method for optical multilayer systems[36]. All the dielectric materials are dispersive, this means that the RI varies with wavelength $n_j = f(\lambda)$. The Lorentz model follows from the classical theory of absorption and despite its simplicity, it offers a good picture of the polarization mechanisms in the material[37]. The optical properties of each layer are characterized completely by the complex dielectric function. The complex dielectric constant and RI are related by: $\varepsilon_j(\omega) = \varepsilon_j^{'} + i\varepsilon_j^{''} = (n_j + ik_j)^2$.

2.3.2 Parameters of SPR Sensors

Throughout this work, several parameters were mentioned to characterize SPR-based sensors. Since the signal used for sensing is the reflected light from the multilayer structure, when analyzing the inherent features of the SPR sensors, some major characteristics of the output optical signal are significant. The various parameters are described in detail in Appendix. A2. There are parameters that governed by the physical properties of the structure, such as sensitivity, dip width, dip depth, low detection limit, and dynamic range. But there are some features that are important on the system level, such as the stability of the sensor within its environment, and the size of the active region.

2.3.3 Methods for Improving SPR Sensor

Since sensitivity is a key feature of SPR sensors, attempts have been made in order to enhance the sensitivity. Improving sensitivity means decreasing the LOD of the system and increasing the ability to detect ultra-small biological and chemical concentration. There are several methods that are based on modifying the basic structure of the KR configuration. Among these methods are: (i) modifying the metal layer composition, (ii) decreasing the prism RI, (iii) adding gratings to the metal layer, (iv) using LR-SPR configuration, and (v) using shaped materials and metamaterials[38;35].

Introducing a modification to KR configuration with ultra-thin dielectric over-layer with high RI can obtain some advantages compared to a conventional SPR sensor. Since the thickness of this film is below the cutoff thickness of the TM_0 mode, this configuration called near guided wave SPR[39] (NGWSPR). It can improve the sensitivity of the sensor, and even boosted by at least two orders of magnitude the effective absorption cross-section of higher harmonics of molecular vibrations[8].

Moreover, when introducing a thick enough dielectric layer one can support guided optical waves, this model called GWSPR conguration so that an asymmetric metal-clad waveguide is produced in which TE and TM modes can exist[39]. The major advantage of this model allows analyzing the material dependent on the polarization of the incident light, which may achieve more information on the molecular structure.

CHAPTER 3

DEVELOPMENT SPR SENSOR

This chapter deal with engineering of two models for SPR biosensor based on the KR configuration by implementing a modification to the conventional structure. In the first model, the NGWSPR configuration used for sensing liquid water with the RI detection method. In the second model, the GWSPR configuration used to detect the molecule vibrational overtone transition with the absorption detection technique. To allow the absorption detection technique, this work focuses on SPR in wavelength interrogation, the incident angle kept fixed and the dip in the optical signal was monitored in the reflectance spectrum.

3.1 High Level System Design

3.1.1 Models

The NGWSPR configuration show in Figure 3.1.a. based on KR configuration which composed of a prism, in our case $45° - 90° - 45°$ made of $SF - 11$ glass, which is coated by a silver layer. The coupling medium, prism, used to match the momentum of a photon with that of surface plasmon in KR configuration. The enhanced electric field on the metal interface due to the surface plasmon excitation boosts the sensitivity of the structure to probe minute changes in the RI of the analyte medium. Although SPR sensors exhibit the highest sensitivity among the sensors due to the evanescent waves, adding a thin dielectric film with high real part of RI on top of the metallic layer significantly enhances the sensitivity of the sensor[36]. Thus I added a thin silicon film on top of the silver layer.

When introducing a thick enough dielectric layer one can support guided optical waves, this model called GWSPR conguration so that an asymmetric metal-clad

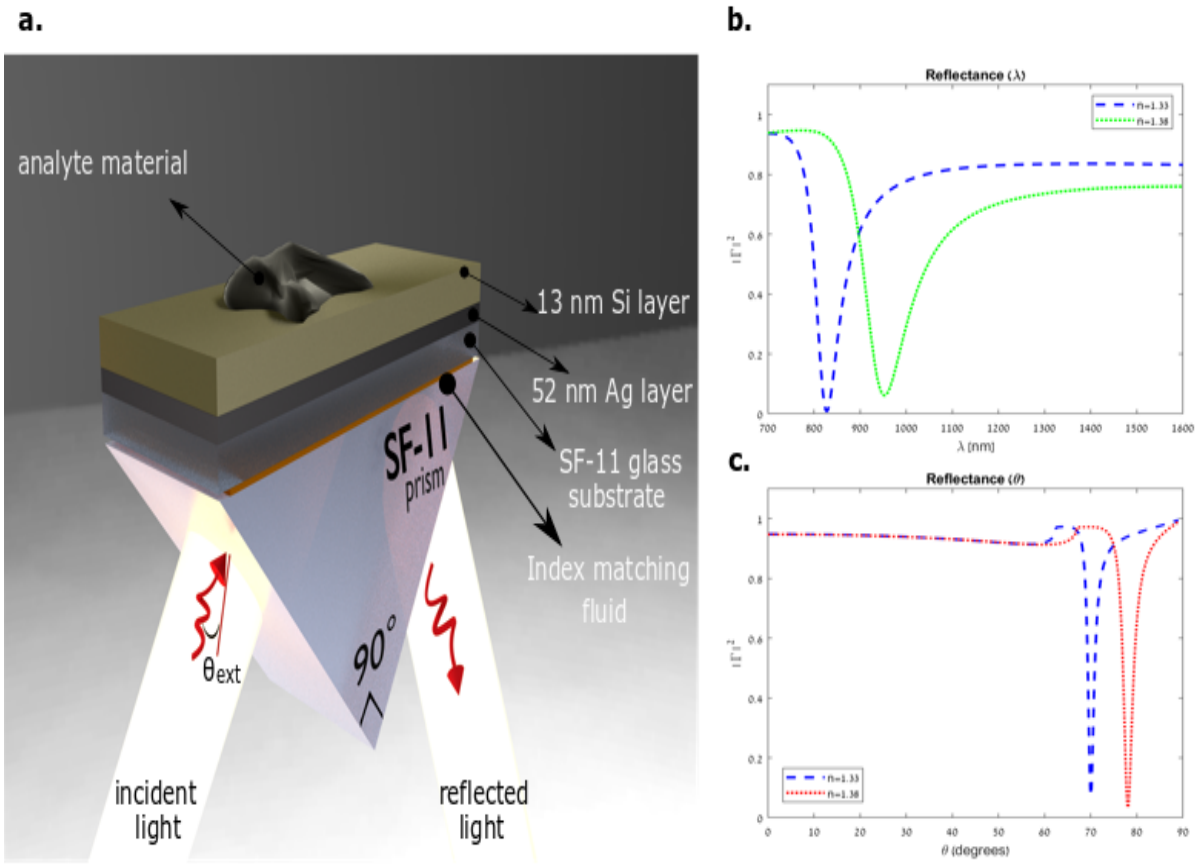

Figure 3.1: NGWSPR configuration: **(a)** Artistic impression of the SPR biosensor model structure based on the KR configuration with adding a dielectric layer on top of the metallic layer. **(b)** Shift of the resonance angle depends on changes in the RI of the analyte medium. **(c)** Shift of the resonance wavelength at a fixed angle of 10° depends on changes in the RI of the analyte medium.

waveguide is produced in which TE and TM modes can exist[39]. Additionally, by coupling the evanescent wave and modes in the silicon layer, one can observe multi-resonance in the reflectivity dip monitored. Finally, adding ultrathin silicon oxide (SiO_2) film over-layer, on both models. The RI of the silicone, act as the core of the waveguide, is higher compared to RI of (SiO_2) which act as cladding, $n_{Si} > n_{SiP_2}$. Hence, strong optical guiding is guaranteed for all signal around the typical near-infrared (NIR) wavelength of $1550nm$. Moreover, this film also protects the sensor from damage caused by the environment.

3.1.2 SPR Numerical Tools

Enhanced the electric field, namely, the evanescent waves which generated from SPR excitation, exhibit high sensitivity of the structure to probe minute changes in the RI of

the analyte medium as shown in Figure 3.1. a and b. Based on the previous chapter, developed a numerical tool for monitored the dip resonance in the reflectance spectrum as a function of angle or wavelength when the condition Equation 2.2 should exist. Code for calculating the reflectance as a function of wavelength provided in Appendix B1, which allows changing the various parameters of the structure such as the thickness of the layers and their dispersion for sensor optimization.

The optical properties of each layer are characterized completely by the complex dielectric function $\varepsilon(\omega)$. Since all the dielectric materials are dispersive, the Lorentz model follows from the classical theory of absorption appears a good picture of the polarization mechanisms in the material. Code for calculating the dispersion relations of the various materials was produced in the Matlab environment and provided in Appendix B2. In the case of metals, the Drude model explains the transport properties of electrons comes from the Lorentz model, which used for silver layer. The Sellmeier equation determines the dispersion of light in the medium such as glasses, which used for $SF-11$ glass prism. To achieving accuracy for silicon and SiO_2 I used an empirical relationship between the RI and wavelength which provide in the database refractiveindex.info[40].

Both models discussed were modeled in the Comsol Multiphysics software in optic waves modeling by considering a small three-dimensional unit cell with a width much smaller than the incident wavelength. This computational model solved Maxwell's equations in the wavelength domain. The simulations can verify the physics and the performance of the sensor which design in MATLAB, in addition, it possible to estimate the field enhancement associated with the excitation of plasmonics resonances.

In general, the figures were provided through this project created with $3D$ computer graphics Blender software and edited using Inkscape software. The calculations were performed in the Matlab environment and simulations were produced in Comsol Multiphysics software, in optic waves modeling.

3.1.3 Sensor Optimization

Since the dispersion in metals is determined mainly by the imaginary part of the refractive index, one may choose a metal type with a low imaginary part to reduce the dispersion and consequently, to obtain a narrower dip in the reflection spectrum. Silver and gold are noble metals that satisfy this condition. The thickness of the metal film was optimized to maximize the efficiency of the excited SPWs with the required wavelength. When this efficiency is maximized, $R_{min}\approx 0$, and the SNR is increasing. To achieve this tuning the thickness of the silver to $52nm$, considering water is the analyte material.

Using silver as the transducer layer has the advantage of high spectral sensitivity but with poor chemical resistance as it deteriorates upon contact with the atmosphere or

some chemicals. Thus, the dielectric layer used as a protection layer responsible for the stability of the sensor usually considered a very important characteristic when the sensor performance needs to be evaluated. The optimal Si thickness was determined using the numerical tools to $13nm$, considering water is the analyte material, in addition, the SiO_2 thickness was defined to $2nm$.

In the case of GWSPR configuration, as a probe molecule, the NMA molecule was used to assess the potential of GWSPR for vibrational overtones enhancement. This molecule constitutes a crucial component of many drugs, pesticides, and explosive[8]. The optimal parameter tuned to achieve resonance at $1490nm$ were the first overtone of the N-H band should appear. The thickness layers were obtained by sweep the simulation with different values, achieving the optimal perpormance with tuning the silver layer to $18nm$, Si to $60nm$, and SiO_2 to $30nm$.

3.2 Low Level System Design

3.2.1 Experimental Set-up

The evanescent field produced at the analyte interface is the major characteristic of the SPR phenomenon it is responsible for the sensing process that occurs in the analyte region. Measuring the changes in the reflected light from the multilayer structure due to the RI changes induced by the molecular interactions can be utilized for sensing and detection. This section deals with the experimental setup, which measures the changes in the intensity of reflected light from an optimal NGWSPR structure as described in the previous chapters for detection water. By obtaining a resonance dip in the profile of the reflectance and compare to calculations, one can sense different materials in real time. The experiment was carried out at '*Light-on-a-Chip*' laboratory which dedicates for exploring, designing, and fabrication of integrated nanophotonic and plasmonic systems.

The schematic in Figure 3.2.a. shows the optical system designed to obtain a correlation between analytical tools and physics that takes place in reality. As an incident plan wave requires a polychromatic source for wavelength interrogation, Stabilized Fiber-Coupled Tungsten light source was used which provide a constant-intensity radiation spectrum from 360 to $2600nm$. Achieving TM polarized coherent light to excite the SPR can with the polarizer was done using a polarizer that was placed after the collimator which connects to the source light with fiber. To match the beam size to pysical size of the prism we used iris light. The light should hit the prism at a fixed angle and go back directly to the detector.

The engineered SPR sensor in this project must be placed on top of the prism, as illustrated in Figure 3.2.a. The $SF-11$ glass substrate of the chip separate from the

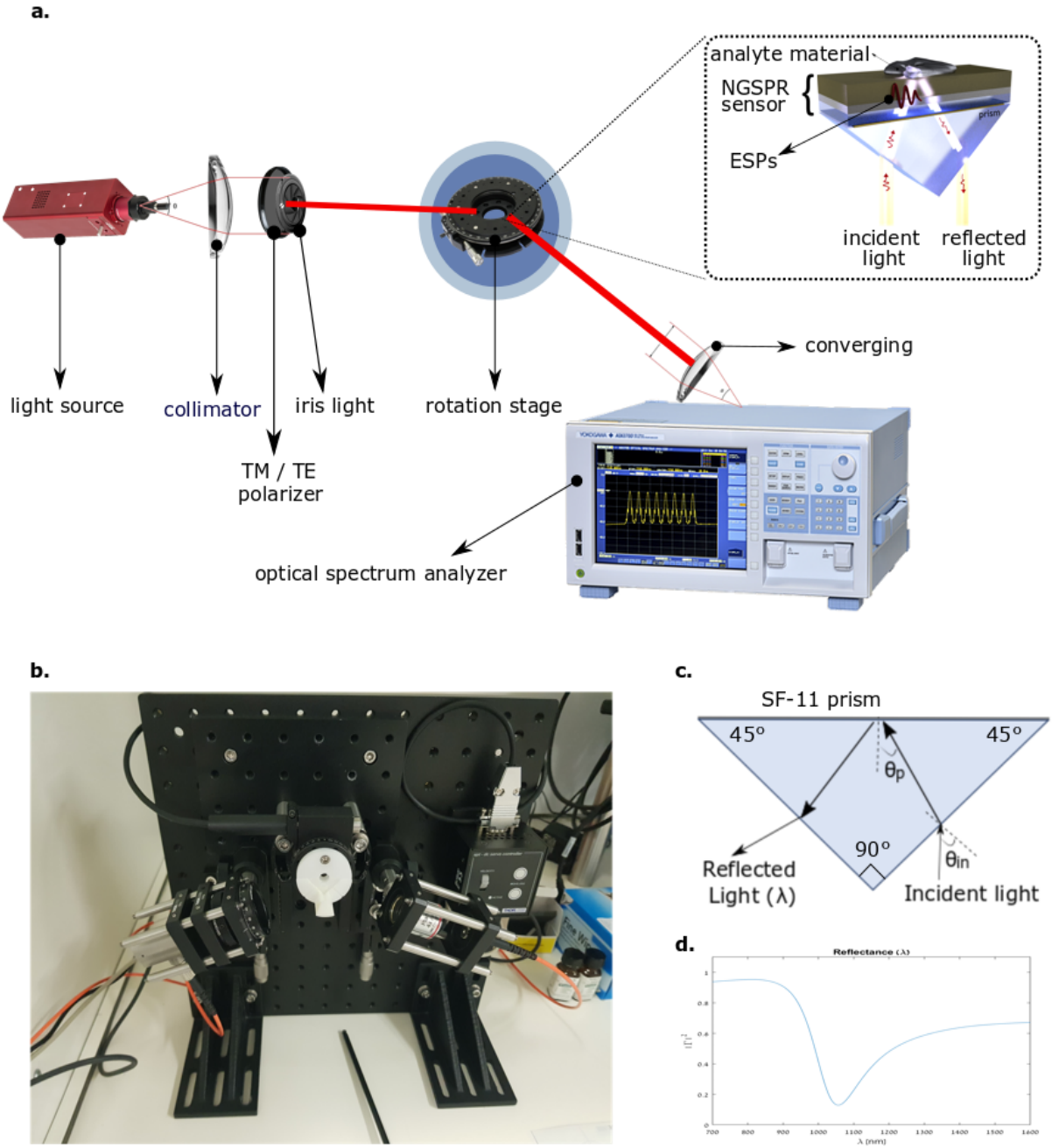

Figure 3.2: Experimental Set-up: **(a)** scheme of the experimental, the beam comes from the light source through a collimator and TM polarizer and then through a iris light, the light hit the prism and reflected directly to the optical spectrum analyzer. The NGWSPR sensor was placed on the prism when the incident light tuned at a fixed angle. **(b)** real image of the optical system. **(c)** geometric of the refraction of light in the prism, the relation between the angle of the incident light θ_{in} and the angle at the metal-prism interface θ_p given by Snell's law. **(d)** calculated reflectance of NGWSPR configuration as a function of wavelength at a fixed angle of 13° when water is the analyte material.

prism by a thin layer of an index-matching fluid with RI approximate to the prism RI at the defined wavelength, namely, $n_{oil}(\lambda = 1500nm) = 1.73$. The thicknesses of the metal and the dielectric layers of the chip were chosen in order to obtain optimal resonance in the NIR region considering that the analyte material is water. A rotation stage with an accuracy of 0.1° was used for measuring the angle θ_{in} of the incident light. The prism located on the stage in such a way that the 180° angle corresponds to the light beam being back-reflected to the light source, this allows us to directly measure the angle. Such a method assumes that both beams cross exactly above the axis of the rotation stage. This can be achieved for a fixed angle only, when several measurements of different angles required to tune the stage before each measure. The optical system was given more clearly by the real image of the optical elements that can be mounted on a common optical bench as shown in Figure 3.2.b.

The reflected light from the NGWSPR structure was collected into a fiber, directly to the optical spectrum analyzer. By converting the reflected beam, in such a way that the fiber area is greater than the section of the light beam, one can focus the beam directly into the fiber. Then, the optical signal was converted to an electric signal, to monitor the dip in the reflectance spectrum.

The measurement of the incident angle defined by the angle between the incident light beam and the normal of the prism surface and oriented according to the counter-clockwise of the plane. Figure 3.2.c show the refraction of light in the prism, to excite the surface plasmon θ_p should match the conditions in Equation 2.2. The relation between the angle of the incident light and the angle at the metal-prism interface can be obtained with the common Snell's law. In the case of $45° - 90° - 45°$ prism, $\alpha = 45°$, with easy geometry, the relation given by:

$$\theta_p = arcsin(\frac{sin\theta_{in}}{n_p(\lambda)}) + \alpha \tag{3.1}$$

The core of the experiment is the measurement of the reflectance of the NGWSPR configuration. In wavelength interrogation, the angle of the incident light kept fixed and the dip is monitored in the reflectance spectrum. One can see in Figure 3.2.d. the obtained resonance dip in the reflectance spectrum at a fixed angle of 13° when water is the analyte material. This result achieved with the numerical tool which engineered in this project for the NGWSPR configuration described in detail in this chapter.

In order to assess the engineering success of NGWSPR sensor, the optical system must be tested. Thus, I probed water as analytical material for comparison between the designed numerical tool and experiment results. I test the system in wavelength interrogation where the angle of incident light was kept fixed, while several different angles tested.

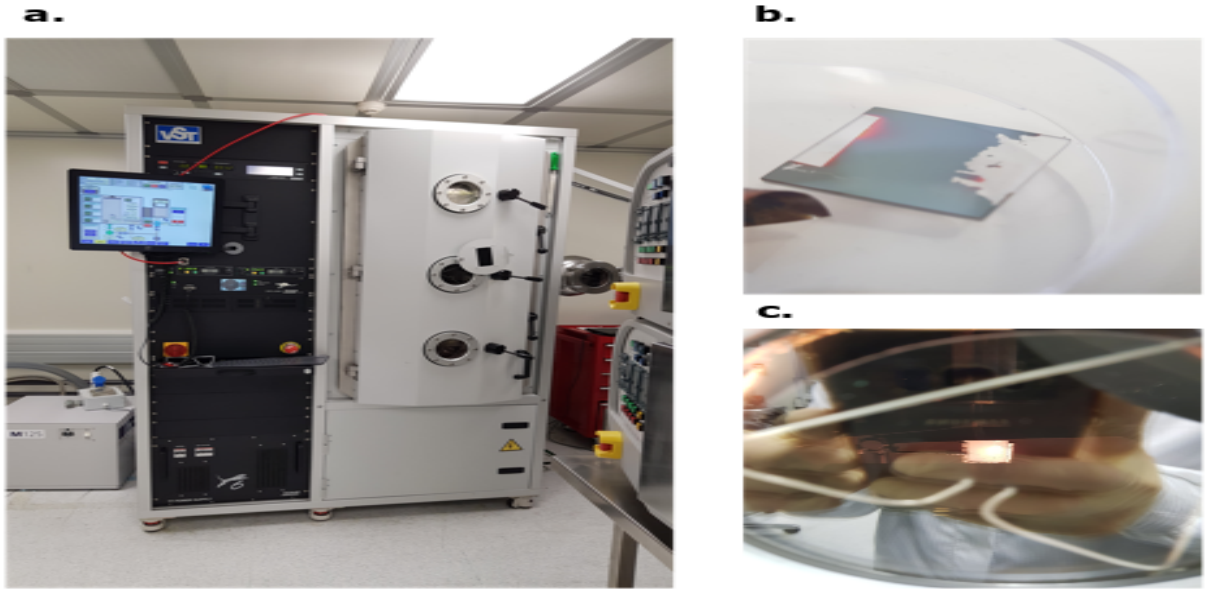

Figure 3.3: The E-beam evaporation process: **(a)** The E-GUN VST system at Nano-Fabrication center. **(b)** The fabricated NGWSPR sample composed of $52nm$ silver, $13nm$ silicon, and $2nm$ SiO_2 films on an SF-11 glass substrate. **(c)** Adding a large amount of energy into the source material by E-beam evaporation process yields a higher density film with increased adhesion to the substrate.

3.2.2 Sensor Fabrication

The thin films deposition of chip sample was carried out with the EBPVD process, in the Nano-fabrication Center at Ben Gurion University. Before using any equipment, I completed training protocol and became a certified user, which including safety training in chemical and biological laboratories, and practical training and certification on the EBPVD system and fulfilling cleanroom work protocol[41].

The fabrication of the chip was done on an SF-11 glass substrate, similar to a prism because the materials cannot deposition directly on the prism due to its physical size and shape limitations. Prior to the fabrication, the N-SF11 glass substrate was solvent cleaned with piranha mixture cleaning for 10 min, and then washed with water. The layers were sequentially e-beam evaporated on the N-SF11 glass substrate by E-GUN VST system shown in Figure 3.3.a. First, silver (Ag) evaporated on the substrate to created $52nm$ film. Next, $13nm$ silicon film deposited and finally, $2nm$ SiO_2 film was deposited.

One can see in Figure 3.3.b. the fabricated NGWSPR sample with the E-beam evaporation process. This process similar to thermal evaporation in the way that source material is heated above its boiling temperature and evaporated to form a film on the surfaces that is stroke by the evaporated atoms[42] there is no chemical reaction which

forms the material on the substrate. In Figure 3.3.c. one can see adding a large amount of energy into the source material with E-GUN VST system which yields a higher density film with increased adhesion to the substrate[42]. More detail on the EBPVD process including a schematic of the general mechanism and figure of the materials were used to fabricate the samples provided in Appendix B3.

CHAPTER 4

RESULTS AND DISCUSSION

4.1 Experiment Results

The NGWSPR model was engineered in such a way that the surface plasmons tuned to resonate at the NIR region, in particular, the wavelength region of 700 to 1600nm. The NIR region characterized by affordable equipment which allows developing low-cost sensor, and mainly the molecular vibrational overtones may appear in this region. Achieving dip in the resonance profile at a defined wavelength can be enabled with the optimal parameters described in detail in the previous chapter. Namely, tuned the silver and silicon layer thicknesses to 52nm and 12nm, respectively. While to exiting the surface plasmons required TM polarized incident light at a higher angle rather the TIR angle in order to fulfill the condition in Equation 2.3. It is more useful to look at the external angle than the angle inside the prism, the relation was simplified by Equation 3.1.

When the incident angle inside the prism is higher than the TIR angle, which is $\theta_{TIR} = 8.34°$ (external angle) in this case, one can achieve SPR considering that water is the analytical material with RI of 1.33. Thus, several angles from 10° to 15° were tested. Figure 4.1.a show colormap of the field distribution by calculating the reflectivity of the NGWSPR structure as a function of both wavelength and incident angle. The colormap is very useful when required to design multilayer structure and examine the performance of the sensor. One can see simply the resonance behavior which is described by the created black curve. The experimental results for each angle described by the stars in the colormap and obtained a great match to the numerical tool. Another idea that comes out of this colormap is that in this configuration with water, only one resonance can be obtained for TM polarization. In this case of NGWSPR configuration, noted that it is not possible to obtain SPR for TE polarization as explained in detail in the analytical

development of the SPR condition in Equation 2.3.

Following the analytical model, when the angle is increased one can expect a left spectral shifting of the resonance dip. It clearly demonstrated in the experimental results shown in Figure 4.1.b. Another point, the dip width of the resonance increases when the resonance wavelength is increased, indicating directly the sensitivity of the sensor. This feature proves the numerical development performed in this project. In the optimization process required $R_{min}\approx 0$ to increase the SNR, during the experiment, an average of $R_{min}\approx 0.1$ was obtained, which attests to the great precision of the fabrication process. This can be explained due to minor nanoscale deviations in the fabrication which changes the thickness of the metal layer, and of course, the effect of heating on dispersion in metals have an additional contribution. Since the dispersion in metals is determined mainly by the imaginary part of the RI, which is responsible for the depth of the obtained resonance, one can be included these effects in the numerical tool for further fabrication.

The completely optical system must be calibrated, thus a comparison between the designed numerical tool and experiment results was performed. This allows further investigation and further fabrication with greater accuracy. This was achieved by changing the optical properties of each layer caused by fabricated the sample using the EBPVD process. The optimal parameters obtained with varying the RI of the silicon layer which given by $n_{Si_{opt}} = 0.7 \cdot n_{Si}$. One can see in Figure 4.2 excellent match between the results from the numerical tool and the obtained measurements. In addition, there was a perfect match between the simulations results in the Comsol Multiphysics software and the Matlab calculations. The NGWSPR sensor which designed shows great detection capability in real time as well as the developed numerical tool extremely accurate.

4.2 GWSPR Simulations

Treating GWSPR configuration start from calculating the dispersion colormaps of the reflectance as a function of both the wavelength and external angle as shown in Figure 4.3. This allows exploring the behavior of the sensor. To achieve SPR at the vibration frequency of the first overtone of N-H band around $\sim 1490nm$, designed GWSPR multilayer structure consisting of $18nm$ silver on an $SF-11$ glass substrate, covered by $60nm$ silicon film and $30nm$ SiO_2. Since the evanescent field decreases when the dielectric layer between the metal and the analyte medium grows, the thickness of the silicon layer was tuned to minimum as possible. On the one hand, when water is the superstrate medium with RI of 1.33 one can see clearly single resonance observed and the TIR angle at $\theta_{TIR} = 8.34°$. On the other hand, when the weakly absorbing homogenous medium presence associated with NMA molecule, multi-resonance appears due to the coupling the evanescent wave and the guided-wave modes in the silicon layer. As opposed

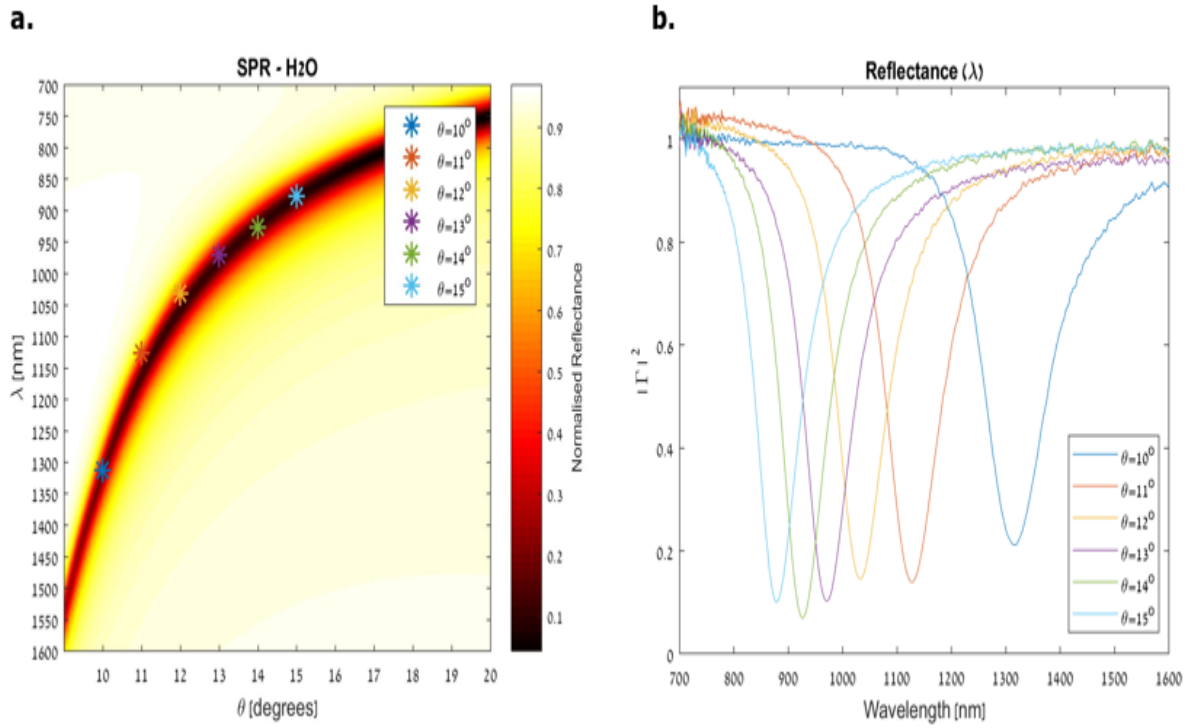

Figure 4.1: Experiment results: **(a)** Calculated results in Matlab of dispersion colormap of NGWSPR multilayer structure with water as a superstrate medium excited by TM polarized light, the experimental results marked with stars. **(b)** obtained reflectance measurements for different incident angles.

to the previous configuration, here, introducing a thick enough dielectric layer which can support guided optical waves, so that an asymmetric metal-clad waveguide is produced in which TE and TM modes can exist. This feature allows exciting SPR with both polarized light TM and TE.

Achieving resonance when $R_{min} \approx 0$ at $1490nm$ using this configuration allows by tuned the external angle of the incident light to 29°. Since the physical size of the prism in the experimental setup required angle as small as possible, which obtained with TE polarized light. The optical system simulated as a unit cell of the multilayer structure to verify the obtained results, as shown in Figure 4.4.a. The simulation results in Figure 4.4.b shows clearly significate field enhancement at the resonance wavelength which tuned to the vibration frecuency of the 1^{st} overtone of N-H band, the results match the expectation. Then code for plotting the dispersion characteristic of pure NMA molecule as a function of the wavelength in NIR region performed as shown in Figure 4.4.c. The orange curve related to the extinction coefficient, the peak at the wavelength around $1490nm$ which corresponds to the first overtone of N-H band.

The DA was calculated according to Equation 1.1 and compare to simulation for

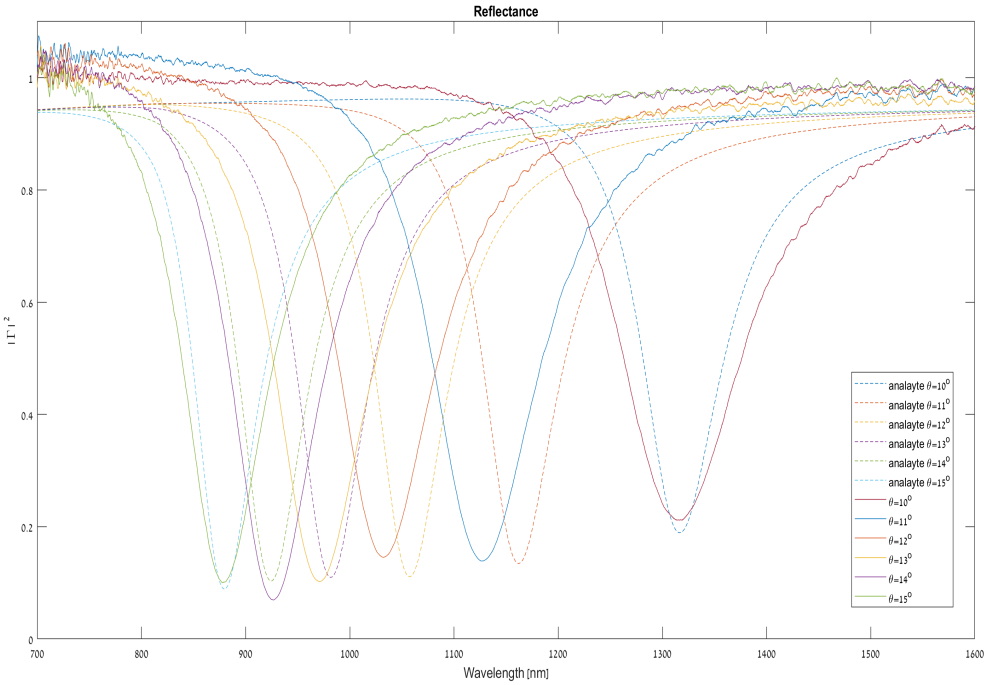

Figure 4.2: Optical system calibration: the reflectance as a function of wavelength measurements (full lines) and numerical results (dashed lines) with calibrating the silicon RI, for TM polarized incident light with different external angles from 10° to 15°.

quantifying the absorption of the vibrational transition overtone due to the interaction with the plasmonic field coupled to guided mode. Firstly, calculate A_{mol} which is the absorption when the pure NMA molecule is present on top of the structure. Whereas A_{BG} is the absorption of the analyte medium considering only the background RI, namely, the A_{BG} is the absorption caused only by the plasmonic field when the vibrational transitions of the molecule are deactivated. When the surface plasmon tuned to resonate exactly at the vibration transition frequency we observed a sharp dip in the DA spectra (dashed-line) as shown in Figure 4.4.d, which match the theory. One can easily recognize the absorption feature of the interrogated band at $1490nm$. The DA signal can exhibit complicated shape due to the interference of the spectrally broad plasmon oscillations with the spectrally narrow molecular vibration[8]. When shifting the plasmonic resonance across the 1^{st} N-H overtone splitting in the DA profile was observed as shown in Figure 4.4.e. In addition, the comparison between the simulation and calculation show great correlation. It is important to note that the effective cross section of pure NMA molecule is enhanced by 4 orders of magnitude when it is detected with the GWSPR configuration.

To better explore the enhancement of the absorption cross section of the molecule using GWSPR configuration, the plasmonic resonance was shifted across the 1^{st} overtone

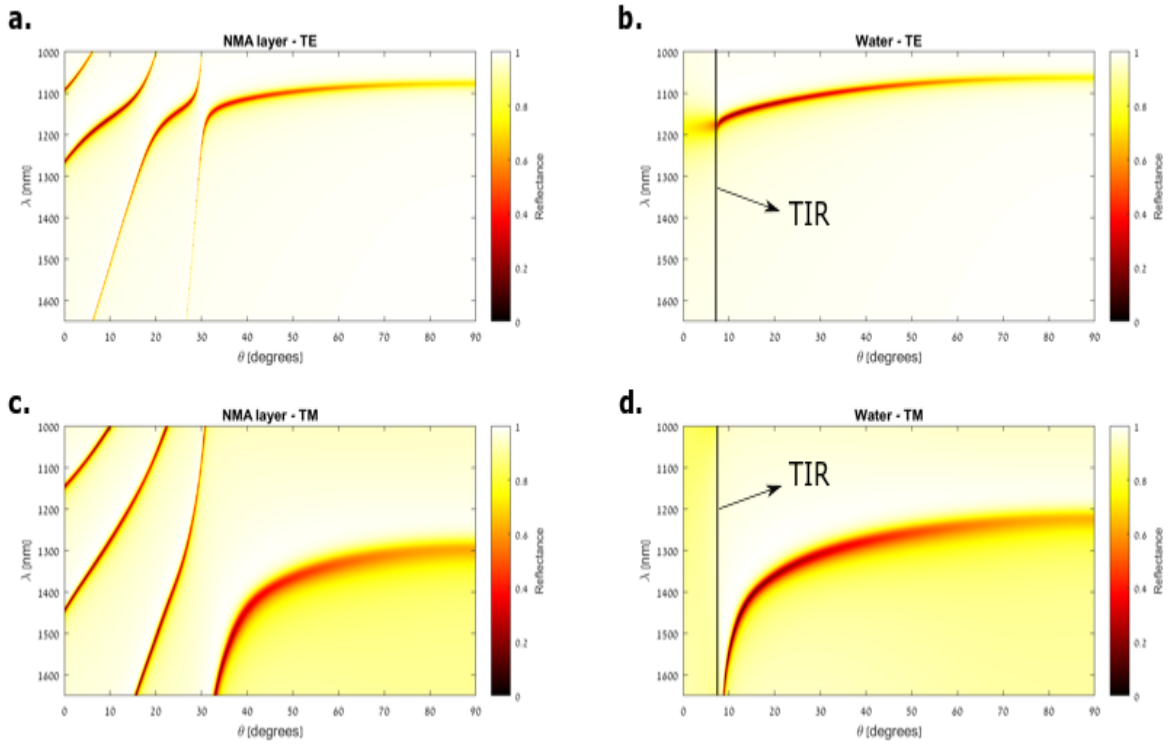

Figure 4.3: GWSPR dispersion colormaps: Calculated GWSPR reflectance as a function of both the wavelength and the incident angle implemented in Matlab, the multilayer structure consisting of $18nm$ silver on an $SF-11$ glass substrate, covered by $60nm$ silicon film and $30nm$ SiO_2. **(a)** the reflectance of a multilayer structure with a superstrate medium of NMA molecule excited by TE polarized light and **(c)** excited by TM polarized light. **(b)** and **(d)** are calculated results in TE and TM respectively of a multilayer structure with water as a superstrate medium with RI of 1.33.

of N-H band. As shown in Figure 4.5 this was achieved by tuning the external angle of the incident light, thus the SPR sweep from $1400nm$ to $1600nm$.

When increasing the angle, left-shift of the resonance observed. As a consequence, DA of the N-H overtone at $1490nm$ changes versus its location with respect to the plasmonic dip. When the molecular absorption band falls on the right shoulder of the SPR dip, it shows splitting in the signal which the dip peaks moving farther and farther away when the molecular band moves to regions where the SPR has larger slopes as can be examined in Figure 4.5.a-b and Figure 4.5.f-g. Whereas smaller signal appears when it is located on the left shoulder of the SPR and the split changed its direction as can be seen in Figure 4.5.d-e and Figure 4.5.i-j. However, DA reaches significantly enhanced and gives a sharp and thin resonance when the vibrational mode matches the SPR wavelength as shown in Figure 4.5.c and Figure 4.5.h.

Further exploring of the interaction between a vibrational overtone and SPR achieved

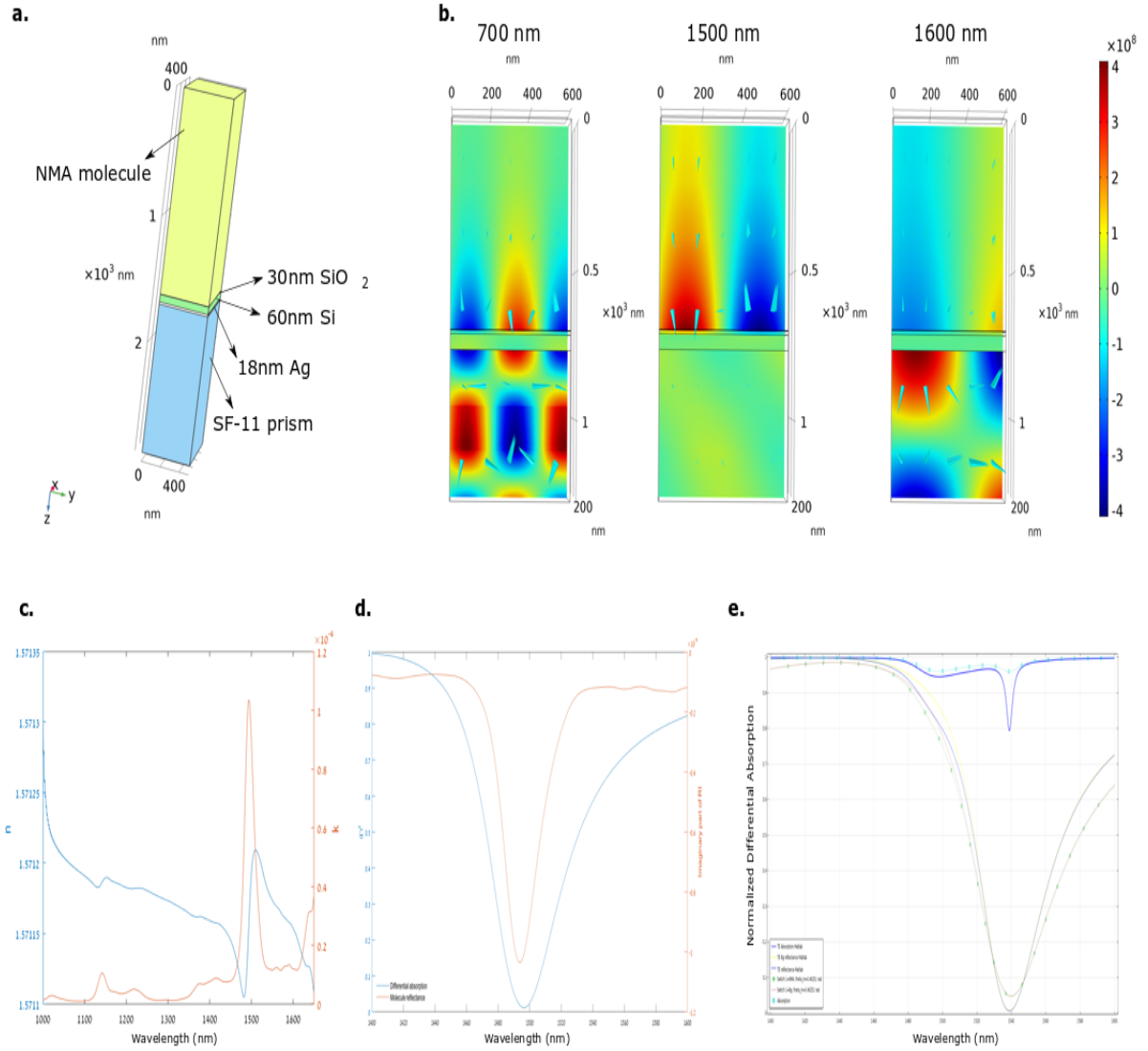

Figure 4.4: Infrared spectroscopy: (a) Schematic of a unit cell 3D simulation model of GWSPR configuration multilayer structure with weakly absorbing homogeneous medium superstrate. **(b)** Evolution of the field enhancement upon plasmon excitation shows the electric field distribution for different wavelengths before (left), after (right) and at the resonance (middle). **(c)** Dispersion characteristic of NMA molecule as a function of the wavelength in NIR region, the imaginary part of RI (blue) and the real part of RI (orange). **(d)** Differential absorption when the SPR is tuned to be in resonance with the absorption N-H band of the first overtone (blue), $\triangle A = |\Gamma_{mol}|^2 - |\Gamma_{BG}|^2$, Comsol simulation and Matlab calculation of reflectance spectra of multilayer structure with (dashed-line) the RI of 1.57 as a superstrate medium and (full-line) when the weakly absorbing homogenous medium presence associated with NMA molecule.

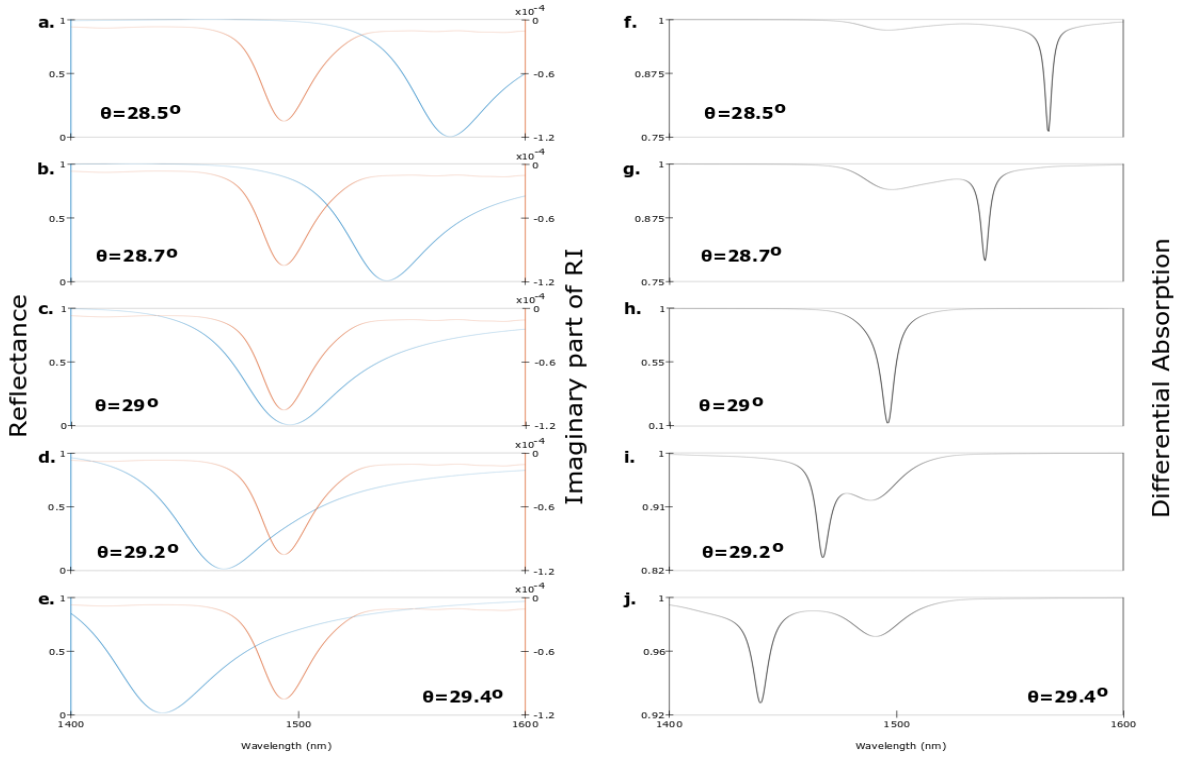

Figure 4.5: Overtone-SPR interaction: (a)–(e) evolution of SPR mode excitation by TE polarized light for different incident angles across the spectrum of the imaginary part of RI of the pure NMA molecule. **(f)-(j)** the corresponding differential absorption calculated for the cases (a)–(e).

with implementing a modification to the conventional dielectric layer. Figure 4.6.a shows the schematic of a unit cell 3D simulation of a perforated silicon layer. The radius of the holes tuned to $150nm$ and the periodic length is $600nm$ between two centers, given that the sizes should be much smaller than the resonant wavelength, approximately 10 times smaller. One can calculate the DA shown in Figure 4.6.b to better explore complex changes in the reflectance spectra. The DA takes both positive and negative values in the spectral range of the first N-H overtone absorption, it shows almost perfect Lorentzian shape. The calculated reflectance when the NMA molecule is present and when considering only the background RI shown in Figure 4.6.c and d respectively. However, the undergoes complex changes in the reflectance profile implying a breaking of the critical angle caused by the discontinuity in the dielectric layer. The positive values of the DA spectra are interpreted as the absorption of the NMA molecules enhanced by exciting surface plasmons. Whereas negative peaks of the DA, occur due to the fast variation of RI in a weakly absorbing medium that leads to the shift of the plasmon band.

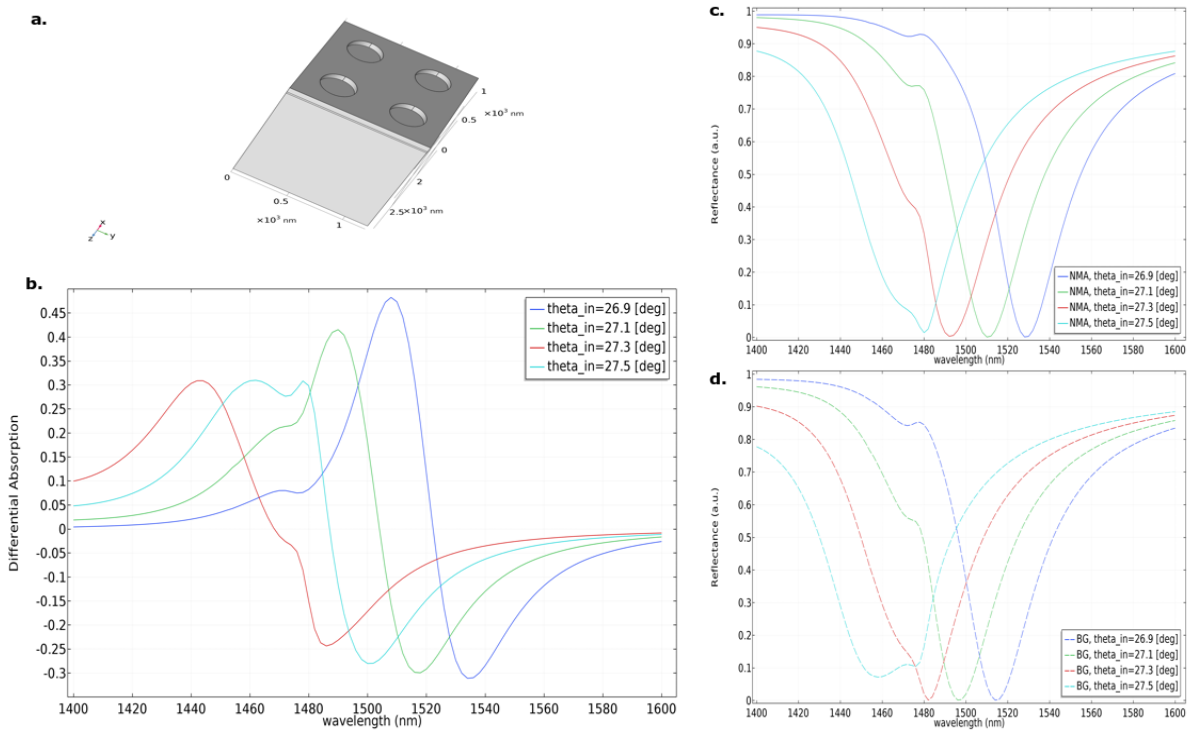

Figure 4.6: Perforated silicon layer in GWSPR configuration : (a) Schematic of a unit cell 3D simulation of GWSPR configuration with a perforated silicon layer. The radius of the holes tuned to $150nm$ and the periodic length is $600nm$ between two centers. **(b)** Differential absorption spectra for different incident angles. **(c)** Calculated reflectance when the NMA molecule is present and **(d)** when considering only the background RI coused only by the plasmonic field.

CHAPTER 5

CONCLUSIONS

To conclude, the development of multilayer structures for molecular detection and sensing based on SPR engineered to operate at NIR wavelengths was presented. This project focus on investigating, design, fabrication, and demonstration of a plasmonics structure used for sensing at real-time by applying SPR properties. Further, a theoretical study of the interaction between molecular vibrational transitions overtones and surface plasmon waves was performed.

Treating SPR physically starts from calculating the dispersion relation of SPWs that can be excited in specific structures. Dispersion colormaps of the reflectance as a function of both the wavelength and external angle was performed which allows exploring the behavior of the sensor. To achieve SPR at the vibration frequency of the first overtone of N-H band around $\sim 1490nm$, designed numerical model.

The system performance characteristics and accuracy are highly dependent on noise. Therefore, the optimal performance was achieved with increasing the SNR by maximizing the efficiency of the exciting SPW.

An NGWSPR sample was fabricated with the EBPVD process. Three layers were sequentially e-beam evaporated on the N-SF11 glass substrate by E-GUN VST system. First, silver evaporated on the substrate to created $52nm$ film. Next, $13nm$ silicon film was deposited and then $2nm$ silicon dioxide film.

To verify the accuracy of the fabrication process, the thickness of the sample was measured as well as spectrum analysis with a spectroscopic ellipsometer was performed.

Experimental setup designed to test the optical system performance. By comparing the measurements with the numerical models, the obtained results of the reflectance spectra match the expectations. This was achieved with accuracy in the theoretical model as well as high quality of fabrication.

Considering the effects of e-beam evaporation on the dispersion relation of materials, in particular the silicon layer, it is required to calibrate the optical system. As exhibited, perfect match obtained between the calculations and the measurements of the reflectance.

To better explore the enhancement of the absorption cross section of the molecule using GWSPR configuration, the plasmonic resonance was shifted across the 1^{st} overtone of N-H band. This was achieved by tuning the external angle of the incident light, thus the SPR sweep from $1400nm$ to $1600nm$. The DA of the N-H overtone at $1490nm$ changes versus its location with respect to the plasmonic dip. When the molecular absorption band falls on the right shoulder of the SPR dip, it shows splitting in the signal which the dip peaks moving farther and farther away when the molecular band moves to regions where the SPR has larger slopes. Whereas smaller signal appears when it is located on the left shoulder of the SPR and the split changed its direction.

However, DA reaches significantly enhanced and gives a sharp and thin resonance when the vibrational mode matches the SPR wavelength. One can elevate the probability of molecular vibrations overtones for detection and sense with enhancing the electric field in which the molecules are embedded. By utilizing the GWSPR configuration, the effective absorption cross-section of vibrational transitions overtones was enhanced by more than two orders of magnitude.

It is important to stress, the observed optical signal can be easily detected by conventional spectrometers having a reasonable SNR, which directly leads to developing a low-cost sensor.

Further exploring of the interaction between a vibrational overtone and SPR achieved with implementing a modification to the conventional dielectric layer with a perforated silicon layer. However, the undergoes complex changes in the reflectance profile implying a breaking of the critical angle caused by the discontinuity in the dielectric layer. Thus the differential absorption takes both positive and negative values in the spectral range around the first N-H overtone absorption, which shows almost perfect Lorentzian shape.

CHAPTER 6

FUTURE PERSPECTIVES

For future continuation of the project, I would like to propose the following ideas: For future continuation of the project, I would like to propose the following ideas:

- New types of shapes for the silicon film should be examined for use in the GWSPR configuration, in order to improve the performance of the sensor. For instance, periodic stripes or even random holes can affect the optical signal.

- One can utilize the nonlinear effects in silicon with the GWSPR configuration for sensing. These effects appear at wavelengths below $1100nm$ which are closer to visible light and may allow detecting higher order of molecular vibrational overtone transitions.

In chapter 2 briefly discussed on the second type of plasmons for noble metal nanostructures, which is the LSPR. In this case, plasmons are sustained by nanoparticles much smaller than the incident wavelength, this gives rise to intense absorption and scattering at their resonance wavelengths. However, recently the coupling configuration between ESPs and LSPR attracted high attention among the researchers due to the extremely enhanced EM field.

Dr. A. Karabchevsky and I investigated the hybrid-dielectric optical system consist of gold nanorods on the top surface of GWSPR configuration. We demonstrated this system for real-time all-optical switch engineered to operate at optical telecommunication wavelengths. Our discovery may open the door for miniature, affordable and ultrafast chip-scale polarization switches as compared to the traditional electronic switches. More details are presented in the abstract on the next page. Due to the impact of this discovery, the work will participate in two conferences:

- *META 2019*, the 10th International Conference on Metamaterials, Photonic Crystals and Plasmonics, 23-26 July 2019, Lisbon, Portugal[43].

- The Batsheva de Rothschild The Israel Science Foundation Research Workshop on: Nonlinear metamaterials and photonic crystals, 9-12 September 2019, Israel[44].

Additionally, the research will be submitted in these days to the prestigious journal publishing *Nature Photonics*.

META 2019

the 10^{th} International Conference on Metamaterials, Photonic Crystals and Plasmonics

Lisbon, Portugal

Metamaterials-based probing weak quantum absorber in coupled three-resonator system with guided wave surface plasmons: sensing or all-optical switching?

By:

Alina Karabchevsky[1,2*] *and Adir Hazan*[1]

[1]Electrooptics and Photonics Engineering Department, Beer-Sheva 8410501, Israel.
[2]Ilse Katz Institute for Nanoscale Science Technology, Center for Quantum Information Science and Technology, Ben-Gurion University of the Negev, Beer-Sheva 8410501, Israel.
*corresponding author, E-mail: alinak@bgu.ac.il

23 – 26 July, 2019

Metamaterials-based probing weak quantum absorber in coupled three-resonator system with guided wave surface plasmons: sensing or all-optical switching?

Alina Karabchevsky[1,2*] and Adir Hazan[1]

[1]Electrooptics and Photonics Engineering Department, Beer-Sheva 8410501, Israel.
[2]Ilse Katz Institute for Nanoscale Science & Technology, Center for Quantum Information Science and Technology, Ben-Gurion University of the Negev, Beer-Sheva 8410501, Israel.
*corresponding author, E-mail: alinak@bgu.ac.il

Abstract

Optical switches selectively switch optical signal from switched-on to switched-off. Compared to the traditional electronic switches, optical switches are not limited by thermal effects or electromagnetic interferences. Here we show metamaterials-based probing of weak quantum absorber in coupled three-resonator system which reveals the signature of optical switching. The polarization dependent probing of molecular overtones excited in a hybrid system tune the state: when the system is illuminated by transverse magnetic polarized light the switch is on while for the transverse electric polarized light the switch is off.

1. Introduction

All-optical switching allows light controls light through unique optical effects. As the field of optical fiber technology has expanded [1], optical switches have been studied and progressed naturally [2,3] giving rise to new configurations such as optically switchable organic light-emitting transistors [4], sub-femtojoule switches [5], plasmonic bandpass filter thermal switches [6], optical control of antiferromagnetic domains [7], utilizing high-mobility of cadmium oxide for ultrafast polarization-controlled [8], multimodal switching of a redox-active macrocycle molecules state toggle [9] active control of anapole states by structuring the phase-change alloy [10] ultrafast optical switching of infrared plasmon polaritons in high-mobility graphene [11]. The efficiency of the switch is defined by its size which dictates the number of input and output ports; switching time of reconfiguration from one state to another; propagation delay time; switching energy to turn on the switch; power dissipation during the switching; crosstalk due to the power leakage to other ports; and physical dimensions [2]. Even though the optical fibers are considered as a pivot of conventional optic telecommunication system [1] their role in switching and processing of photonic signals is limited and fulfilled by electronics. Here we report on all-optical switch due to the excitation of molecular overtones in hybrid plasmonic-dielectric configuration. By coupling of photons with the conductive charges at the metal-dielectric interface, plasmonics gives rise to nanoscale optical devices operating at sub-wavelength regime [13]. Hybrid plasmonic-dielectric configuration possesses a unique property to controlling the switch with polarization state of light that allows two different plasmonic modes co-exist while exciting single molecular overtone absorption band. Due to the possibility of developing energy efficient, real-time analyzing, and ultra-compact components at an affordable cost, plasmonics may be the next arrangement in optical communications. Despite the fact that many plasmonics-based applications appeared, such as sensors [14], detectors, modulators, switches, and microwave components, no attempts were done so far to designing all-optical hybrid plasmonic-dielectric switching systems based on effect of excitation of forbidden molecular overtones transitions.

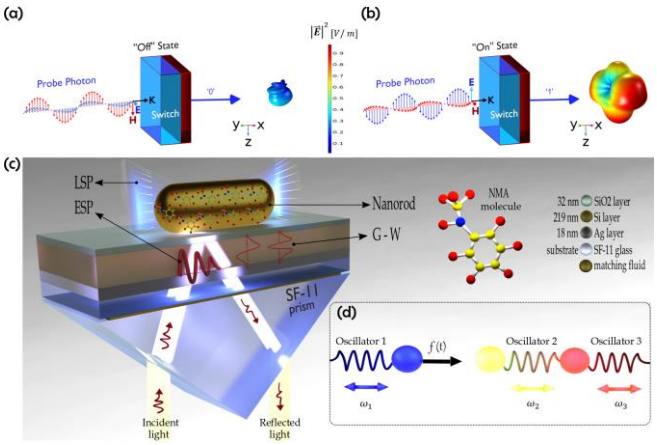

Figure 1: (a) Schematic illustration of polarized beam incident the switch. The state 'off' is activated when the TE polarized beam hits the switch, (b) the state 'on' is activated when the TM polarized light hits the switch. (c) Artistic representation of experimental setup. (d) Mechanism of coupled oscillators.

2. Results and Discussion

Here we study on all-optical switch due to the excitation of molecular overtones in hybrid plasmonic-dielectric configuration. Figure 1 illustrates the concept of the system based on molecular excitation under TE and TM polarized light. In the state 'off', Figure 1a, TE polarized light is being transmitted through the medium. Figure 1b illustrates state 'on' in which TM polarized light excites molecular overtone transition resulting in a well-defined resonance due to the strong light absorption. Calculated far-field radiation diagrams in subplots Figure 1a and Figure 1b show the directivities for each state. At lower wavelengths however, excited molecular signatures experience different response to the incident light under TE and TM polarizations.

Figure 1c shows the modeled and tested experimentally system in which polarized incident polychromatic light illuminates the facet of the prism. Thin film composed of silicon on silver is placed on the prism with matching oil. N-Mathylaniline molecule is dripped on the surface of the film together with gold nanorods. Light hits the base of the prism and penetrates through the thin film while exciting the guided modes. Guided modes in turn excite the molecular overtones. The energy transfer occurs between the molecular overtone vibrations to the localized surface plasmon excited in nanorod. We treat the coupling between the guided wave-to overtone-to localized surface plasmon as a system with three coupled oscillators having eigenfrequencies $\boldsymbol{\omega_{1,2,3}} = \sqrt{\frac{k_{1,2,3}}{m_{1,2,3}}}$, $\boldsymbol{\omega_1}$, $\boldsymbol{\omega_2}$ and $\boldsymbol{\omega_3}$ coupled together with coupling spring constants $\mathbf{k_1}$, $\mathbf{k_2}$ and $\mathbf{k_3}$ and masses $\mathbf{m_1}$, $\mathbf{m_2}$ and $\mathbf{m_3}$. Figure 1d shows the oscillating mechanism of the system. Oscillator 1 is the guided mode surface plasmon, oscillator 2 is the molecular overtone vibration and oscillator 3 is the localized surface plasmon oscillator. The oscillators requirement is extremely demanding.

3. Conclusions

In summary, we explored the system in which three coupled oscillators are excited. Despite the relatively low oscillator strength of the corresponding forbidden dipole transition in harmonic oscillator approximation we constructed an optical switching system based on polarization depending properties of the plasmon-to-overtone coupled modes. This all-optical switching manifold is realized by excited localized surface plasmons (LSP) which couple to the molecular vibrations overtones. LSP in the system are excited by the extended surface plasmons (ESP) which in turn are excited by the guided modes of a waveguide structure.

References

1 Midwinter, J. E. Trends in optical fibre transmission research. Nature 261, 371-376 (1976).

2 Saleh, B. E. & Teich, M. C. Fundamentals of photonics. (john Wiley & sons, 2019).

3 Midwinter, J. E. Photonics in switching. (Academic Press, 2012).

4 Hou, L. et al. Optically switchable organic light-emitting transistors. Nature Nanotechnology, doi:10.1038/s41565-019-0370-9 (2019).

5 Nozaki, K. et al. Sub-femtojoule all-optical switching using a photonic-crystal nanocavity. Nature Photonics 4, 477, doi:10.1038/nphoton.2010.89 https://www.nature.com/articles/nphoton.2010.89#supplementary-information (2010).

6 Sun, M. et al. A Photonic Switch Based on a Hybrid Combination of Metallic Nanoholes and Phase-change Vanadium Dioxide. Scientific Reports 8, 11106, doi:10.1038/s41598-018-29476-6 (2018).

7 Manz, S. et al. Reversible optical switching of antiferromagnetism in TbMnO3. Nature Photonics 10, 653, doi:10.1038/nphoton.2016.146 https://www.nature.com/articles/nphoton.2016.146#supplementary-information (2016).

8 Yang, Y. et al. Femtosecond optical polarization switching using a cadmium oxide-based perfect absorber. Nature Photonics 11, 390, doi:10.1038/nphoton.2017.64 https://www.nature.com/articles/nphoton.2017.64#supplementary-information (2017).

9 Payne, D. T. et al. Multimodal switching of a redox-active macrocycle. Nature Communications 10, 1007, doi:10.1038/s41467-019-08978-5 (2019).

10 Tian, J. et al. Active control of anapole states by structuring the phase-change alloy Ge2Sb2Te5. Nature Communications 10, 396, doi:10.1038/s41467-018-08057-1 (2019).

11 Ni, G. X. et al. Ultrafast optical switching of infrared plasmon polaritons in high-mobility graphene. Nature Photonics 10, 244, doi:10.1038/nphoton.2016.45 https://www.nature.com/articles/nphoton.2016.45#supplementary-information (2016).

12 Barnes, W. L., Dereux, A. & Ebbesen, T. W. J. n. Surface plasmon subwavelength optics. 424, 824 (2003).

13 Karabchevsky, A., Mosayyebi, A. & Kavokin, A. V. Tuning the chemiluminescence of a luminol flow using plasmonic nanoparticles. Light: Science & Applications 5, doi:doi: 10.1038/lsa.2016.164 (2016).

CHAPTER 7

APPENDICES

APPENDIX A

A1 Molecular Vibrational Transitions

Molecular overtone bands are bands observed in the vibrational spectrum of an anharmonic oscillator along with the fundamental band arising as a result of the transition $\triangle v = \pm 1$. Whereas the overtones arising as a result of the transition $\triangle v = \pm 2$ and $\triangle v = \pm 3$ for 1^{st} and 2^{nd} overtones, respectively, and so on. The intensities of the overtones are a few orders smaller than the fundamental vibrational transitions, in approximate 1/10 and 1/100 of the intensity of the fundamental band for the 1^{st} and 2^{nd} overtones, respectively. Figure 1 show diagrams of an oscillator mechanism described by the energy levels and the corresponding spectral transmittance patterns for various oscillators.

The mechanism of the EM radiation absorption can be explained by the example shown in Figure 2. It illustrates a white beam source emitting light of multiple wavelengths which is focused on a sample. Upon striking the sample, photons that match the energy gap of the molecules present, green light in this example, are absorbed in order to excite the molecule. Other photons transmit unaffected and, if the radiation is in the visible region $400 - 700nm$, the sample color is the complementary color of the absorbed light. By comparing the attenuation of the transmitted light with the incident, an absorption spectrum can be obtained.

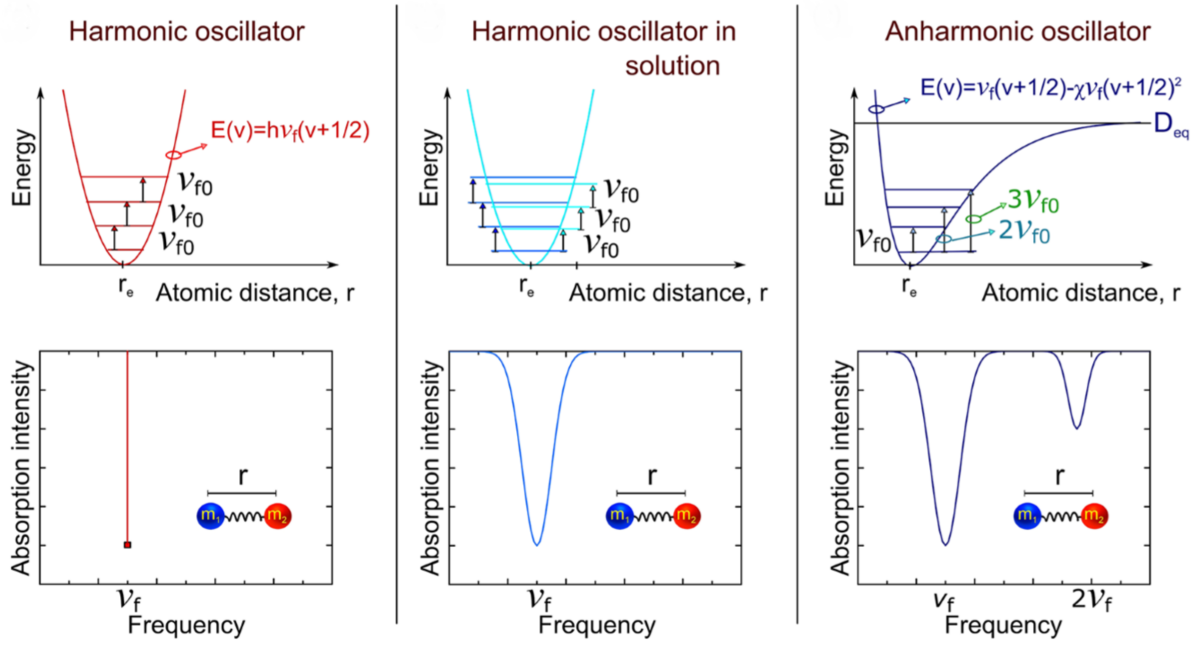

Figure 1: Diagrams of an oscillator mechanism[28]: described by the energy levels (top) and the corresponding spectral transmittance patterns (bottom).

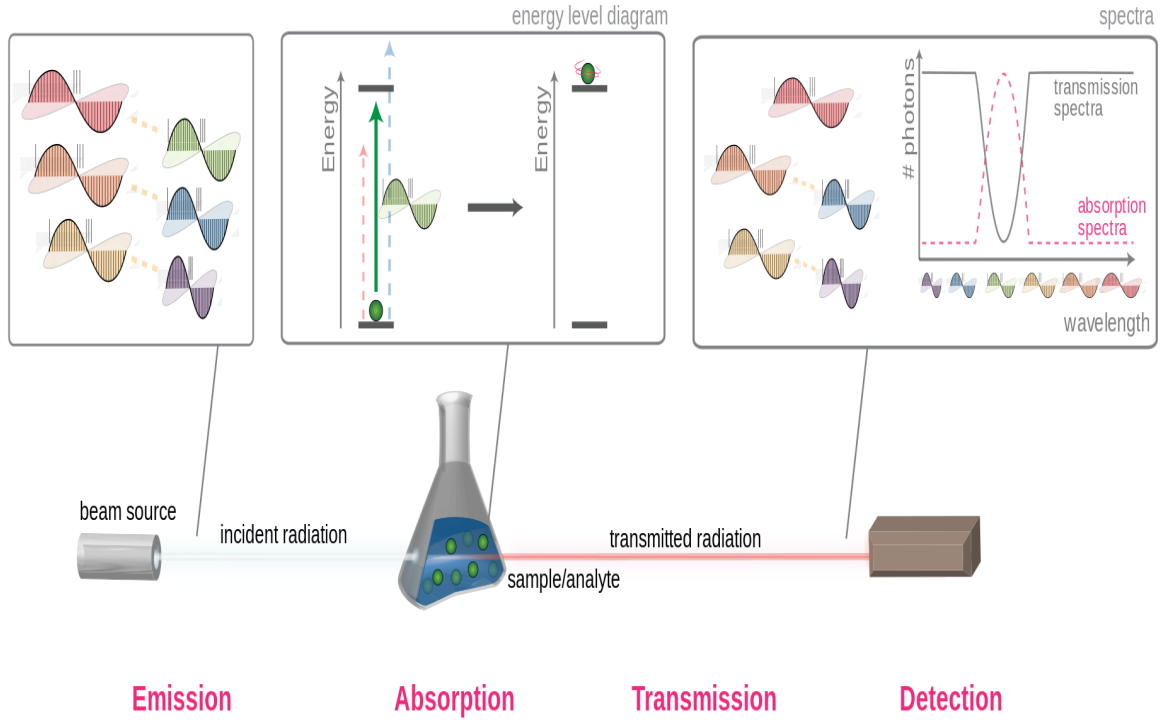

Figure 2: Mechanism of the EM radiation absorption[33].

A2 Definitions of SPR Parameters

Definitions of the various parameters mentioned in this work refer to definitions as written in the methodology[35], whether the angular or the spectral interrogations are used:

Sensitivity is defined as the ratio between the shifts in the parameter that is being monitored and the proper change in the analyte RI. This simple definition is given by: $S_\lambda \equiv \frac{d\lambda}{dn_a}$. The expressions of the spectral and angular sensitivities show that this sensitivity strongly depends on the physical structure of the sensor, such as the RI of a prism, in addition to the incident light properties such as the incidence angle and wavelength. The physical origin of improving the sensitivity of SPR sensors is by enhancing the EM intensity inside the analyte.

Dip width is simply the full width half maximum (FWHM) of the reflectivity profile. The importance of the FWHM lies in that it determines the accuracy of the measurement. The smaller the width of the dip, the higher the capability of the system to deduce small variations in the analyte medium. The width of the dip is governed by the propagation distance of the plasmons at the interface between the metal and the analyte.

Dip depth is the contrast of the measurement which refers to the relative portion of the incident light that has experienced the resonance effect. This parameter depends on both the sensor design and the definition of the incident light. Since the SPR phenomenon can be understood by means of interference effects from a thin film, the thickness of the layers should be designed appropriately in order to enhance the strength effects.

Penetration depth of the EM field inside the analyte is another important feature of SPR sensors, although it cannot be deduced directly from the reflectance profile. It shows how far the EM field can vertically penetrate into the analyte. In principle, the entire region extended within the penetration depth can be sensed by the field, which acts as the sensor probe. Hence, larger penetration depth means larger sensing strip. Since this distance is on the order of a few hundreds of nanometers in conventional SPR sensors, these sensors are able to monitor events that are very close to the surface. This characteristic, which does not solely depend on the structure but also on the excitation features, is of high importance when the sensing target contains large molecules. In addition, the penetration depth indirectly correlates with the sensitivity of the sensor.

Low detection limit (LOD) combines both the sensitivity and the resolution of the system. The LOD is the smallest quantity of change in the analyte RI (or translated into concentration) that can be detected by the optical system. The LOD is determined both by the sensitivity and the noise level of the sensor as a system: $LOD = \triangle\zeta_{min}/S_\zeta$ where defining ζ as the change in the information parameter related to the SPR signal, S_ζ is the sensitivity corresponding to the parameter ζ , and $\triangle\zeta_{min}$ is the minimum detectable change in the measurement, usually taken to be the value of the noise level.

APPENDIX B

B1 Code for calculating the reflectance of NGWSPR structure by Matlab

```
function R = MultiLayer(n,L,lambda,theta,pol)

%-------------------------------------------------------
% Input
%-------------------------------------------------------
% 'n'      = vector of refractive indices
% 'L'      = vector of optical lengths of layers
% 'lambda' = vector of free-space wavelengths
% 'theta'  = incidence angle from left medium (in degrees)
% 'pol'    = 'tm' or 'te', for parallel/perpendicular polarizations
%
%-------------------------------------------------------
% Output
%-------------------------------------------------------
% 'R': Reflectance


% Number of layers
M = length(n)-2;

% Single interface, no slabs
```

```
if M==0, L = []; end
theta = theta * pi/180;
costh = sqrte(1 - (n(1) * sin(theta) ./ n).^2);

if strcmp(pol,'te') || strcmp(pol,'TE')
    % Transverse refractive indices
    nT = n .* costh;
else
    % TM case, fails at 90 deg for left medium
    nT = n ./ costh;
end

if M>0
    % n(i)*l(i)*cos(th(i))
    L = L .* costh(2:M+1);
end

% r(i) = (n(i-1)-n(i)) / (n(i-1)+n(i))
r = -diff(nT) ./ (diff(nT) + 2*nT(1:M+1));

% Initialize R at right-most interface
R = r(M+1) * ones(1,length(lambda));
for i = M:-1:1
    % Phase thickness in i-th layer
    delta = 2*pi*L(i)./lambda;
    z = exp(-2*1i*delta);
    R = (r(i) + R.*z) ./ (1 + r(i)*R.*z);
end

R=abs(R).^2;
end
```

B2 Code for calculating the dispersion relations of different materials by Matlab

```
function [dis,n,L]=dispersion(lambda,d)

%-----------------------------------------------
% Input
%-----------------------------------------------
% lambda - vector of wavelengths in [nm]
% d - vector of layer thicknesses in [nm]
%
%-----------------------------------------------
% Output
%-----------------------------------------------
% 'dis': Structure containing material dispersion
% 'n': vector of refractive index
% 'L': vector of Optical thickness


%% SF11: Sellmeier
b=[1.73759695 0.313747346 1.89878101];
c=[0.013188707 0.0623068142 155.23629];

dis.SF11(:,1)=lambda;
dis.SF11(:,2)=sqrt(1 ...
                + (b(1).*(lambda*1e6).^2) ./ ((lambda*1e6).^2-c(1)) ...
                + (b(2).*(lambda*1e6).^2) ./ ((lambda*1e6).^2-c(2)) ...
                + (b(3).*(lambda*1e6).^2) ./ ((lambda*1e6).^2-c(3)));

%% Ag: Drude-Lorentz
%LD: Drude-Lorentz model for the complex dielectric constant of metals
dis.Ag(:,1)=lambda;
[~,~,dis.Ag(:,2)] = LD(lambda,'Ag','LD');
dis.Ag(:,2)=conj(dis.Ag(:,2));

%% Experimental Si and SiO2
Si=importdata('Si.txt');
```

```
dis.Si(:,1)=lambda;
dis.Si(:,2)=spline(Si(:,1),Si(:,2),lambda*1e9)...
    -1i*spline(Si(:,1),Si(:,3),lambda*1e9);

SiO2n=importdata('SiO2.txt');
dis.SiO2(:,1)=lambda;
dis.SiO2(:,2)=spline(SiO2n(:,1),SiO2n(:,2),lambda*1e9);

%% Pure NMA
n_NMA=importdata('n_100%NMA.txt');
dis.n_NMA(:,1)=lambda;
dis.n_NMA(:,2)=spline(n_NMA(:,1)*1e9,n_NMA(:,2),lambda*1e9)...
    -1i*spline(n_NMA(:,1)*1e9,n_NMA(:,3),lambda*1e9);

%% Create required structures for simulation
na = dis.SF11(:,2);
np = dis.Ag(:,2);
n1 = dis.Si(:,2);
n2 = dis.SiO2(:,2);
nb =1.33*ones(length(lambda),1);
n = [na, np, n1, n2, nb];

% Optical Thickness
Lp = n(:, 2)*d(1)./(lambda*1e9);
L1 = n(:,3).*d(2)./(lambda*1e9);
L2 = n(:,4).*d(3)./(lambda*1e9);
L = [Lp, L1, L2, L3];
end
```

B3 Electron Beam-Physical Vapor Deposition (EB-PVD)

Vapor deposition is useful techniques to fabricating different materials. In general, there are two types of deposition: physical vapor deposition (PVD) and chemical vapor deposition (CVD). Here, we use the electron beam-physical vapor deposition (EB-PVD), the material deposited physically, namely, moved to the top of a substrate without chemical reaction. E-beam evaporation is a process similar to thermal evaporation in such a way that source material is heated above its boiling temperature and evaporated to form a film on the surfaces that is stroke by the evaporated atoms.

A cleanroom is not enough! evaporation takes place in a vacuum. Figure 3.a represents schematically the general mechanism of EB-PVD process[42]. With the source material placed in the crucible, a filament below the crucible is heated. By applying a large voltage, electrons are drawn from the filament and focused as a beam on the source material by several bending magnets. The beam is swept across the surface of the source material to heat all of the material. One can see in Figure 3.b the material which used for fabricating our sample with E-GUN VST system at Nano-Fabrication center[41].

There are a few advantages of e-beam evaporation over thermal evaporation, for instance, the possibility to add a larger amount of energy into the source material which yields a higher density film with increased adhesion to the substrate[42;41]. In addition, E-beam only heats the source material and not the entire crucible, a lower degree of contamination from the crucible will be present than in the case of thermal evaporation. It is possible to deposit several different materials without breaking the vacuum by using a multiple crucible E-beam gun.

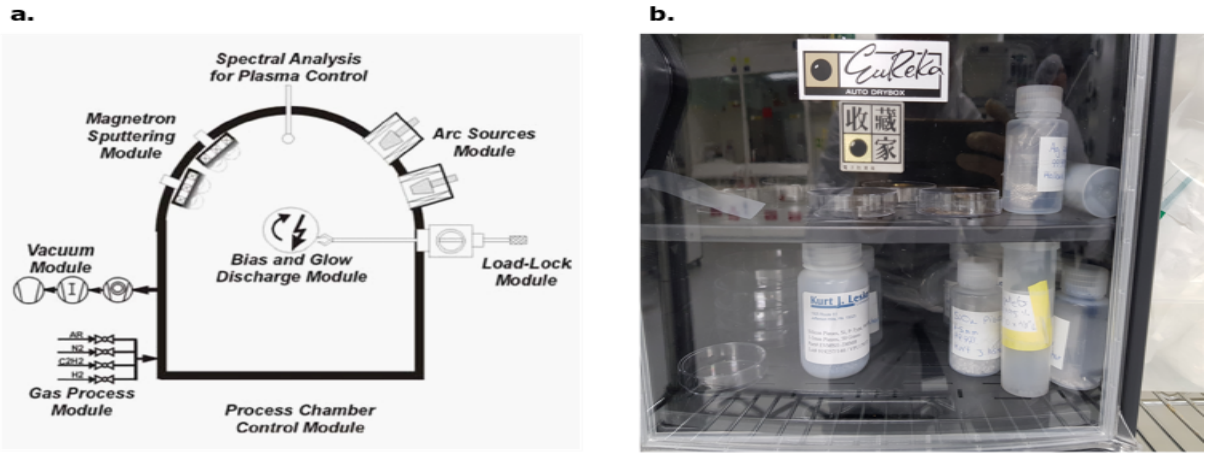

Figure 3: E-beam evaporation: (a) the general mechanism of EB-PVD process[42]. **(b)** the used materials for NGWSPR sample fabrication (Ag, Si, and SiO_2) by E-GUN VST system[41].

REFERENCES

[1] F. S. Ligler and C. R. Taitt, *Optical biosensors: today and tomorrow.* Elsevier, 2011.

[2] R. Peltomaa, B. Glahn-Martínez, E. Benito-Peña, and M. Moreno-Bondi, "Optical biosensors for label-free detection of small molecules," *Sensors*, vol. 18, no. 12, p. 4126, 2018.

[3] B. Špačková, P. Wrobel, M. Bocková, and J. Homola, "Optical biosensors based on plasmonic nanostructures: a review," *Proceedings of the IEEE*, vol. 104, no. 12, pp. 2380–2408, 2016.

[4] B. Stuart, "Infrared spectroscopy," *Kirk-Othmer Encyclopedia of Chemical Technology*, pp. 1–18, 2000.

[5] H. W. Siesler, Y. Ozaki, S. Kawata, and H. M. Heise, *Near-infrared spectroscopy: principles, instruments, applications.* John Wiley & Sons, 2008.

[6] C. N. Banwell, E. M. McCash *et al.*, *Fundamentals of molecular spectroscopy.* McGraw-Hill New York, 1994, vol. 851.

[7] A. Karabchevsky and A. Kavokin, "Giant absorption of light by molecular vibrations on a chip," *Scientific reports*, vol. 6, p. 21201, 2016.

[8] A. Karabchevsky and A. Shalabney, "Strong interaction of molecular vibrational overtones with near-guided surface plasmon polariton," in *Optical Sensing and Detection IV*, vol. 9899. International Society for Optics and Photonics, 2016, p. 98991T.

[9] J. P. Camden, J. A. Dieringer, J. Zhao, and R. P. Van Duyne, "Controlled plasmonic nanostructures for surface-enhanced spectroscopy and sensing," *Accounts of chemical research*, vol. 41, no. 12, pp. 1653–1661, 2008.

[10] P. Berini, "Long-range surface plasmon polaritons," *Advances in optics and photonics*, vol. 1, no. 3, pp. 484–588, 2009.

[11] H. Raether, *Surface plasmons on smooth and rough surfaces and on gratings*. Springer-Verlag Berlin An, 2013.

[12] V. M. Shalaev and S. Kawata, *Nanophotonics with surface plasmons*. Elsevier, 2006.

[13] I. Abdulhalim, M. Zourob, and A. Lakhtakia, "Surface plasmon resonance for biosensing: a mini-review," *Electromagnetics*, vol. 28, no. 3, pp. 214–242, 2008.

[14] Y. Zeng, R. Hu, L. Wang, D. Gu, J. He, S.-Y. Wu, H.-P. Ho, X. Li, J. Qu, B. Z. Gao *et al.*, "Recent advances in surface plasmon resonance imaging: detection speed, sensitivity, and portability," *Nanophotonics*, vol. 6, no. 5, pp. 1017–1030, 2017.

[15] R. Adato, S. Aksu, and H. Altug, "Engineering mid-infrared nanoantennas for surface enhanced infrared absorption spectroscopy," *Materials today*, vol. 18, no. 8, pp. 436–446, 2015.

[16] R. Adato and H. Altug, "In-situ ultra-sensitive infrared absorption spectroscopy of biomolecule interactions in real time with plasmonic nanoantennas," *Nature communications*, vol. 4, p. 2154, 2013.

[17] D. R. Dadadzhanov, T. A. Vartanyan, and A. Karabchevsky, "Vibrational overtones spectroscopy enabled by plasmonic nanoantennas," in *Plasmonics: Design, Materials, Fabrication, Characterization, and Applications XVI*, vol. 10722. International Society for Optics and Photonics, 2018, p. 107222E.

[18] S. J. Orfanidis, "Electromagnetic waves and antennas," 2002.

[19] A. Shalabney and I. Abdulhalim, "Electromagnetic fields distribution in multilayer thin film structures and the origin of sensitivity enhancement in surface plasmon resonance sensors," *Sensors and Actuators A: Physical*, vol. 159, no. 1, pp. 24–32, 2010.

[20] E. L. Hu, M. Brongersma, and A. Baca, "Applications: nanophotonics and plasmonics," in *Nanotechnology Research Directions for Societal Needs in 2020*. Springer, 2011, pp. 417–444.

[21] M. C. Roco, C. A. Mirkin, and M. C. Hersam, *Nanotechnology research directions for societal needs in 2020: retrospective and outlook*. Springer Science & Business Media, 2011, vol. 1.

[22] S. Ghoshal, M. Sahar, M. Rohani, and S. Sharma, "Nanophotonics for 21st century," in *Optoelectronics-Devices and Applications*. IntechOpen, 2011.

[23] M. David and M. Florescu, *BIOMOLECULAR INTERACTION EVALUATION USING SURFACE PLASMON RESONANCE. SPR BIOSENSORS, in: Biophysics for Biomedical and environmental Sciences, Transilvania University Press, Brasov, 2016.*, 01 2016, pp. 211–223.

[24] J. Yang, *Novel chemistry turns conventional polymers into biomedical supermaterials. PHYS ORG*, 10 2014.

[25] W. Peng, Y. Liu, P. Fang, X. Liu, Z. Gong, H. Wang, and F. Cheng, "Compact surface plasmon resonance imaging sensing system based on general optoelectronic components," *Optics express*, vol. 22, no. 5, pp. 6174–6185, 2014.

[26] S. Romano, G. Zito, S. Manago, G. Calafiore, E. Penzo, S. Cabrini, A. C. De Luca, and V. Mocella, "Surface-enhanced raman and fluorescence spectroscopy with an all-dielectric metasurface," *The Journal of Physical Chemistry C*, vol. 122, no. 34, pp. 19 738–19 745, 2018.

[27] K. Kant and S. Abalde-Cela, "Surface-enhanced raman scattering spectroscopy and microfluidics: Towards ultrasensitive label-free sensing," *Biosensors*, vol. 8, no. 3, p. 62, 2018.

[28] A. Katiyi and A. Karabchevsky, "Si nanostrip optical waveguide for on-chip broadband molecular overtone spectroscopy in near-infrared," *ACS sensors*, vol. 3, no. 3, pp. 618–623, 2018.

[29] W. Bai, H. Yang, Y. Ma, H. Chen, J. Shin, Y. Liu, Q. Yang, I. Kandela, Z. Liu, S.-K. Kang *et al.*, "Flexible transient optical waveguides and surface-wave biosensors constructed from monocrystalline silicon," *Advanced Materials*, vol. 30, no. 32, p. 1801584, 2018.

[30] M. Iodice, L. De Stefano, G. Coppola, V. Mocella, I. Rea, E. De Tommasi, E. Orabona, and I. Rendina, "Label-free biosensing by means of optical micro-ring resonator," in *Optical Sensors 2009*, vol. 7356. International Society for Optics and Photonics, 2009, p. 735603.

[31] A. Karabchevsky, A. Katiyi, M. I. M. Bin Abdul Khudus, and A. V. Kavokin, "Tuning the near-infrared absorption of aromatic amines on tapered fibers sculptured with gold nanoparticles," *ACS Photonics*, vol. 5, no. 6, pp. 2200–2207, 2018.

[32] S. Robinson and N. Dhanlaksmi, "Photonic crystal based biosensor for the detection of glucose concentration in urine," *Photonic Sensors*, vol. 7, no. 1, pp. 11–19, 2017.

[33] Wikipedia, "Absorption spectroscopy," https://upload.wikimedia.org/wikipedia/commons/f/f2/Spectroscopy_overview.svg, 2011, [8-January -20011].

[34] I. Abdulhalim, "Coupling configurations between extended surface electromagnetic waves and localized surface plasmons for ultrahigh field enhancement," *Nanophotonics*, vol. 7, no. 12, pp. 1891–1916, 2018.

[35] A. Shalabney and I. Abdulhalim, "Sensitivity-enhancement methods for surface plasmon sensors," *Laser & Photonics Reviews*, vol. 5, no. 4, pp. 571–606, 2011.

[36] C. C. Katsidis and D. I. Siapkas, "General transfer-matrix method for optical multilayer systems with coherent, partially coherent, and incoherent interference," *Applied optics*, vol. 41, no. 19, pp. 3978–3987, 2002.

[37] K. E. Oughstun and N. A. Cartwright, "On the lorentz-lorenz formula and the lorentz model of dielectric dispersion: addendum," *Optics express*, vol. 11, no. 21, pp. 2791–2792, 2003.

[38] J. Zhang and L. Zhang, "Nanostructures for surface plasmons," *Advances in Optics and Photonics*, vol. 4, no. 2, pp. 157–321, 2012.

[39] A. Lahav, M. Auslender, and I. Abdulhalim, "Sensitivity enhancement of guided-wave surface-plasmon resonance sensors," *Optics Letters*, vol. 33, no. 21, pp. 2539–2541, 2008.

[40] refractiveindex.info, "Refractive index database," https://refractiveindex.info/, [].

[41] T. N.-F. Center, "The Nano-Fabrication center at Ben-Gurion university," https://in.bgu.ac.il/en/nano-fab/Pages/default.aspx, [].

[42] D. Zhang, "Thermal barrier coatings prepared by electron beam physical vapor deposition (eb–pvd)," in *Thermal barrier coatings*. Elsevier, 2011, pp. 3–24.

[43] M. 2019, "the 10th International Conference on Metamaterials, Photonic Crystals and Plasmonics," https://metaconferences.org/ocs/index.php/META19/META19#.XQWDpLxvZPY, 23-26 July 2019, [Lisbon, Portugal].

[44] T. B. de Rothschild The Israel Science Foundation Research Workshop on:, "Nonlinear metamaterials and photonic crystals," https://lmicenter.wixsite.com/nonlinearseminar2019, 9-12 September 2019, [Israel].

- This project was written with LaTeX.
- Artistic impression of the experimental was created with 3D computer graphics Blender software.
- The calculations were performed in the Matlab environment.
- Simulations were produced in COMSOL Multiphysics software, in optic waves modeling.

פיתוח מבנים רב-שכבתיים לחיישנים ביולוגים מבוססי תהודת פלזמון משטחי

דו״ח מסכם

מאת:

אדיר חזן

בהנחיית:

ד״ר אלינה קרבצבסקי & ד״ר משה זוהר

SCE
SHAMOON COLLEGE OF ENGINEERING

 # 108

המכללה האקדמאית ע״ש סמי שמעון
המחלקה להנדסת חשמל ואלקטרוניקה
באר שבע

פיתוח מבנים רב-שכבתיים לחיישנים ביולוגים מבוססי תהודת פלזמון משטחי

מאת:
אדיר חזן

בהנחיית:
ד״ר אלינה קרבצבסקי
ד״ר משה זוהר

דו״ח מסכם

פרויקט הנדסי המוגש לשם השלמת הדרישות לקבלת תואר ראשון במדעים B.Sc.

סיון , תשע״ט
יוני 2019

SCE
SHAMOON COLLEGE OF ENGINEERING

תקציר

פיתוח מבנים רב שכבתיים מבוססי תהודת פלזמון משטחי (תפ״מ) עבור חיישה וזיהוי מולקולרי הינה תכליתו העיקרית של פרויקט זה. חדשנותו המרכזית של הפרוייקט נעוצה בגילוי מדעי אשר ממנו עולה כי בכדי להגביר את המעברים הויברציאוניים המולקולריים בתחום האינפרא-אדום הקרוב, ניתן לעשות שימוש בתכונות התפ״מ על-ידי תכנון והנדסת מבנים רב-שכבתיים בקנה מידה הננומטרי. לצורך כך, יעמיק הפרוייקט בחקירת ובהנדסת המבנה, החל בתכנון תיאורטי, אופטימיזציה שלו, וכלה בייצור החיישן. לאחר קבלת המוצר המוגמר תבחן הצלחתו במסגרת ביצוע ניסוי חישה בזמן אמת.

בשלב התכנוני של המבנה יושם דגש על המרכיב העיקרי של המערכת האופטית שהינו השבב המשמש לחיישה. בהתבסס על המתודולוגיה הנוכחית, בעבודה זו בוצע פיתוח חיישן בתצורת - NGWSPR. פיתוח חדשני זה הושג בעזרת יישום שינוי למבנה הקונבנציונאלי של Kretschmann-Raether, וזאת על ידי הוספת שכבה דיאלקטרית דקה על גבי המשטח העליון של המבנה. לצורך השגת התכלית המרכזית שהינה מימוש ביצועי מערכת אופטימליים הושם דגש רב בתיכנון החיישן. במסגרת תכנונו של החיישן, בוצעו סימולציות אשר בהתאם לתוצאותיהן, ייצרנו את הדגם המבוקש וזאת במסגרת תהליך מורכב של נידוף פיזיקלי העושה שימוש באלומת אלקטרונים (EBPVD). לבסוף, ועל מנת לוודא כי תכונותיו של החיישן הינן משביעות רצון, היה צורך בבדיקת המערכת תוך ביצוע ניסויים ומדידות והשוואתן למודלים המספריים.

כאשר עובי השכבה הדיאלקטרית די עבה ניתן לתמוך בגלים אופטיים מודרכים, תצורה זו נקראת GWSPR, אשר פחות ידועה במתודולוגיה. היעד הנוסף והאחרון של עבודה זו היה לבחון באופן תיאורטי את הפוטנציאל של מודל GWSPR עבור זיהוי מעברים מולקולרים באמצעות טכניקת ׳שיפור משטח ספיגת האינפרא-אדום׳ (SEIRA). לשמחתנו יצויין כי, גם יעד זה הושג בהצלחה ועימו המסקנה החד משמעית בדבר קיומו של פוטנציאל כביר בזיהוי מעברים מולקולרים תוך שימוש בתצורה זו.

פרוייקט זה היווה בסיס התחלתי להמשך מחקר מעמיק אשר בוצע על ידי ד״ר אלינה קרבצבסקי ואנוכי במסגרתו חקרנו את המערכת האופטית דיאלקטרית-היברידית המורכבת ממוטות בקנה מידה ננומטרי העשויות זהב על פני המשטח העליון של מודל ה- GWSPR והראנו כי, מערכת זו יכולה לשמש עבור מתגים אופטיים בזמן אמת המהונדסים לפעול באורכי גל המאופיינים בתקשורת אופטית. תגלית זו עשויה לפתוח דלת עבור מתגי קיטוב מיניאטורים, זולים הפועלים במהירות גבוהה לעומת המתגים האלקטרונים המסורתיים הקיימים כיום. בשל החדשנות של גילוי זה, המחקר ישתתף בשני כנסים ומוגש בימים אלה לפרסום בכתב העת היוקרתי *Nature Photonics* ועוד יביא עימו סימן לבאות.

מילות מפתח: מבנים פלזמונים, חיישנים ביולוגים אופטיים, תהודה פלזמונית משטחית, ספקטרוסקופיה באינפרא-אדום.

עבודה זו בוצעה בקבוצת המחקר *'אור-על-שבב' בניהולה של* ד"ר אלינה קרבצבסקי, במחלקה להנדסת אלקטרו-אופטיקה ופוטוניקה, אוניברסיטת בן גוריון, באר שבע.

סוג הפרויקט: מחקר

תחומי הפרויקט: פוטוניקה משולבת ,פלזמונים, חיישנים ביולוגים אופטיים, ננוטכנולוגיה, ספקטרוסקופיה באינפרא-אדום.

פיתוח מבנים רב-שכבתיים לחיישנים ביולוגים מבוססי תהודת פלסמון משטחי

דו"ח מסכם

פרויקט הנדסי המוגש לשם השלמת הדרישות לקבלת תואר ראשון במדעים B.Sc.

מאת:
אדיר חזן

בהנחיית:
ד"ר אלינה קרבצבסקי
ד"ר משה זוהר

המכללה האקדמית להנדסה ע"ש סמי שמעון
המחלקה להנדסת חשמל ואלקטרוניקה
באר-שבע

סיון , התשע"ט
יוני 2019

חתימות המנחים:

Alina Karabchevsky
ד"ר אלינה קרבצבסקי

Moshe Zohar
ד"ר משה זוהר

חתימת הסטודנט:

Adir Hazan
אדיר חזן, 203156559

תאריך: _____ **אישור ועדת הפרויקטים:** _____